CFD STUDY OF TURBO-RAMJET INTERACTIONS IN HYPERSONIC AIRBREATHING PROPULSION SYSTEM

FINAL REPORT

ING CHANG
PRAIRIE VIEW A&M UNIVERSITY
PRAIRIE VIEW, TEXAS

LOUIS G. HUNTER
LOCKHEED MARTIN-TACTICAL AIRCRAFT SYSTEMS
FORT WORTH, TEXAS

SEPTEMBER, 1996

PREPARED FOR
NASA/LEWIS RESEARCH CENTER
UNDER CONTRACT NAG3-1500

TABLE OF CONTENTS

Abstract

Advanced airbreathing propulsion systems used in Mach 4-6 mission scenarios, usually involve turbo-ramjet configurations. As the engines transition from turbojet to ramjet, there is an operational envelope where both engines operate simultaneously.

In the first phase of our study, an over/under nozzle configuration was analyzed. The two plumes from the turbojet and ramjet interact at the end of a common 2-D cowl, where they both reach an approximate Mach 3.0 condition and then jointly expand to Mach 3.6 at the common nozzle exit plane. For the problem analyzed, the turbojet engine operates at a higher nozzle pressure ratio than the ramjet, causes the turbojet plume overpowers the ramjet plume, deflecting it approximately 12 degrees downward and in turn the turbojet plume is deflected 6 degrees upward. In the process, shocks were formed at the deflections and a shear layer formed at the confluence of the twojets. This particular case was experimentally tested and the data were used to compare with a CFD study using the PARC2D code. The CFD results were in good agreement with both static pressure distributions on the cowl separator and on nozzle walls. The thrust coefficients were also in reasonable agreement. In addition, inviscid relationships were developed around the confluence point, where the two exhaust jets meet, and these results compared favorably with the CFD results.

In the second phase of our study, A 3-D CFD solution was generated to compare with the 2-D solution. The major difference between the 2-D and 3-D solutions was the interaction of the shock waves, generated by the plume interactions, on the sidewall. When a shock wave interacts with a sidewall and sidewall boundary layer, it is called a glancing shock sidewall interaction. These interactions entrain boundary layer flow down the shockline into a

vortical flow pattern. The 3-D plots show the streamlines being entrained down the shockline. The pressure of the flow also decreases slightly as the sidewall is approached. Other difference between the 2-D and 3-D solutions were a lowering of the nozzle thrust coefficient value from 0.9850 (2-D) to 0.9807 (3-D), where the experimental value was 0.9790.

In the third phase of our study, a different turbo-ramjet configuration was analyzed. The confluence of a supersonic turbojet and a subsonic ramjet in the turbine-based-combined-cycle (TBCC) propulsion system was studied by a 2-D CFD code. In the analysis, Mach 1.4 primary turbojet was mixed with the subsonic ramjet secondary flow in an ejector mode operation. Reasonable agreements were obtained with the supplied 1-D TBCC solutions. For low downstream backpressure, the Fabri choke condition (Break-Point condition) was observed in the secondary flow within mixing zone. For sufficient high downstream backpressure, the Fabri choke no longer exist, the ramjet flow was reduced and the ejector flow became backpressure dependent. Highly non-uniform flow at ejector exit were observed, indicated that for smooth downstream combustion, the mixing of the two streams probably required some physical devices.

1. Introduction

For hypersonic vehicles, the propulsion could come from either turbojet nozzle or ramjet nozzle, or both. At low speed flight, the propulsion is solely from turbojet nozzle. While at high speed flight, the propulsion could be all from ramjet nozzle. During the transition, both nozzles could be in operation. When the two nozzle flows are combined to form a single exit, the resulting compressible, turbulent flow will be very complex. It requires the most advanced computational fluid mechanics (CFD) program to analyze the flow fields. In this research project, the main objective is to use the proper CFD tools to obtain 2-D or 3-D solutions and compared the results with the supplied experimental data or the simplied 1-D control volume solutions.

Two types of turbo-ramjets configurations were studied in this report. The first one is the so called over/under turbo-ramjets. In this configuration, the turbojet is housed in an upper bay with a separate ramjet housed in a lower bay. As the engines transited from turbojet mode to ramjet mode, there is an operational envelope where both engines operate simultaneously. The confluence of the two jets then jointly expand to high Mach number through a common nozzle. The other turbo-ramjets configuration studied is the so called turbine-based-combined-cycle (TBCC) propulsion system. It is a version of the tandem turbo-ramjets configuration, where a bypass duct is separated from the turbomachine by a splitter plate. This duct feeds part of the inlet flow to the ramburner downstream of the turbine exhaust, where the mixed flow exits from a single nozzle.

The first phase of the research was a 2-D CFD study of the over/under nozzle flows, which will be discussed in Chapter 2. In the study, the grids were generated by GRIDGEN2D

code. The flow solver used was the PARC2D code with K-KL two-equation turbulence model. The output solutions were plotted on computer graphics in both line forms and contour plots by using PLOT3D code. The solutions were compared with wind tunnel data supplied by NASA/Lewis Research Center. The CRAY supercomputer was used for the computations.

In the second phase of the research, the CFD study was extended to 3-D over/under nozzle flow analysis. The task addressed the 3-D block grid generation and the execution of a 3-D full Navier-Stoke flow solver (HAWK). The output solutions were plotted on computer graphics by using PLOT3D. The results were compared with 2-D CFD solutions. The detailed discussion is in Chapter 3 of this report.

For the third phase of the research, a different turbo-ramjets configuration was studied. The system consisted of a turbine engine housed in an upper bay with a splitter plate underneath, which separates the lower ramjet flowpath. For certain range of engine operation, a relatively low Mach number flow was in the bypass duct, the splitter plate did not completely isolate the primary turbojet flowpath from the bypass flowpath (the lower ramjet flowpath), and resulting in ejector type flow interactions between the two streams. In addition, a ramjet spraybar was configured to burn the remaining oxygen in both the primary and secondary streams. The heat addition was also metered to chocked the flow thermally. The CFD study included the grid generation by using GRIDGEN2D Code, and the flowfield solutions by using a 2-D FALCON flow solver. The 2-D CFD results were compared with control volume results (from 1-D TBCC solutions) supplied by NASA/Lewis Research Center. Details of this phase of research is discussed in Chapter 4.

2. Over/Under Nozzle CFD Study and Comparison with Data-Two Dimensional Analysis

2.1 INTRODUCTORY REMARK

High speed vehicles have great value in reconnaissance, interdiction and strike missions (Reference 1). Other applications include cruise missiles and hypercruisers with the possibilities of civil transportation. High speed vehicle design concepts are complicated by propulsion components which have definite limits in terms of speed and altitude. Typically turbojets are only effective up to Mach numbers of approximately 3, ramjets from 3-6 and scramjets from Mach 6-15. For a Mach 6 vehicle, there is a requirement for a dual engine concept which can be integrated into an annular configuration or over-under concepts typically houses the turbojet in an upper bay and ramjet in the lower bay (Figure 2.1), where this figure shows an integrated design with movable doors on both the inlet and nozzle. Over a range of Mach numbers, both engines run simultaneously, their exhaust jets interacting with one another, causing some losses as shocks are formed when the jets mutually interact with each other. The turbojet mass flow and nozzle pressure ratio (NPR) is greater than the ramjet, for the case under consideration, which causes the ramjet plume to be dominated by the turbojet plume causing some angularity and shock losses.

Another phenomena of interest here, is the effect of small radii nozzle throats, which create over expansions followed by recompression waves, just downstream of the throats. These waves enter the nozzle flowfield, creating pressure anomalies on the nozzle walls as they reflect and interact with the complicated integrated flowfield downstream. These anomalies show up in the data, especially on the walls.

Nozzle wall pressure distributions and thrust coefficients were compared with the data (Reference 2). For the single nozzle configuration this procedure is well defined, however there are some issues when dealing with multinozzles.

2.2 FLOW SOLVER

The code used in this work was the PARC 2-D code (Reference 3) with enhancements and k-kl turbulence model (Reference 4). The k-kl turbulence model solves two turbulent transport equations, one for turbutlent kinetic energy (k) and the second for the quantity (kl) where l is the turbulent length scale. The k-kl turbulence model features advanced formulations for positive and negative pressure gradients along with wall functions, which allows grid spacing near the wall to be somewhat relaxed, with y-plus values up to 300. For this study a y-plus value of 14 was used.

Low Reynolds number applications, require somewhat more restrictive y-plus values (Reference 5), as well as other two equation turbulence models (Reference 6 and 7), which result in a large number of grid points. This requirements does cause some concerns when dealing with large multi block configurations.

2.3 CONFIGURATION

The 2DCD Over-Under Mach 3.0 configuration is shown in Figure 2.2. The upper turbojet nozzle is composed of relatively sharp throat radii shown in the inset, while the lower nozzle has sharp nozzle radii only on the bottom surface where the upper nozzle surface is relatively flat. The dimension L9 shown in Figure 2 is the reference length for all X/Lref dimensionless length scales. The confluence point referred to in this report is at the exit plane of

A9 and A19. Three blocks were used to grid the configuration, with grid 1 and grid 2 having 123 x 55 points each and grid 3 (formed beginning at the A9 and A19 exit plane to the end of the integrated nozzle plane B-H) with 109 x 110 points. The total number of grid points is 25,520 with 55 points across each throat. The software used for grid generation is GRIDGEN2D.

2.4 CFD RESULTS

2.4.1 Convergence

A flow solution is considered to be converged, when the L2 residual falls six orders of magnitude in 5,000 iterations (Figure 2.3). In addition, the mass flows from each nozzle (CFD) are used to determine convergence, when the compound massflow approaches a steady value. It is interesting to note that the ramjet massflow converges more quickly than the turbojet massflow, because the nozzle has only one throat radii and the upper nozzle surface is basically flat. Massflows computed at A9 and A19 as well as at each corresponding throat, indicate stable converged equal massflow values at 5,000 iterations (Figure 2.4 and 2.5). These massflows are per unit width.

2.4.2 Formation of Shocks at the Confluence Point

As the two supersonic nozzle flows meet at the confluence point (Figure 2.6), the mutual interaction causes the turbojet streamlines (Figure 2.7) to deflect approximately 6 degrees and the ramjet streamlines 12 degrees. The sum of these angles adds up to the cowl angle of 18 degrees. The inviscid solution for M1 = 2.9, M2 = 3.0, P1/P2 = 1.33, is δ_1 = 6.8 degrees, ε_1 = 25.3 degrees, δ_2 = 11.2 degrees and ε_2 = 28 degrees. The CFD solutions for these conditions show an initial streamline turning angle of 12 degrees on the ramjet side and shock angle of approximately 28 degrees then growing steeper as it moves away from the confluence point. In

addition, the higher turbojet pressure causes the streamlines to separate on the ramjet cowl side just before the confluence plane. On the turbojet side, the streamline turn 6 degrees with the shock angle near 25 degrees, which agrees well with the inviscid theory. The initial conditions M1 = 2.9, M2 = 3.0, P1/P2 = 1.33 were taken from the CFD converged solutions. The inviscid governing equations at the confluence point for $\gamma = 1.4$ are as follows:

$$\left(\frac{7M_1^2\sin^2\varepsilon_1-1}{6}\right)-\left(\frac{7M_2^2\sin^2\varepsilon_2-1}{6}\right)\frac{P_2}{P_1}=0 \qquad (1)$$

$$\frac{1}{\tan\delta_1}-\left(\frac{1.2M_1^2}{M_1^2\sin^2\varepsilon_1-1}-1\right)\tan\varepsilon_1=0 \qquad (2)$$

$$\frac{1}{\tan\delta_2}-\left(\frac{1.2M_2^2}{M_2^2\sin^2\varepsilon_2-1}-1\right)\tan\varepsilon_2=0 \qquad (3)$$

$$\delta_1+\delta_2=18 \qquad (4)$$

where 18 degrees represents the nozzle cowl angle.

Even though the CFD equations are fully viscous, the boundary layers are relatively thin as well as the shear layer, with the result that the CFD is in relatively good agreement with the inviscid theory at the confluence point.

2.4.3 Formation of Shocks Just Downstream of Nozzle Throats

The formation of oblique shocks just downstream of axisymmetric nozzle throats has received considerable attention in the past, both experimentally (Reference 8) and computationally (References 9 and 10). The cause stems from the flow expanding rapidly just downstream of the throat due to the throat's small radius of curvature. The high angular

momentum must be reduced to meet the tangential wall boundary condition, which is accomplished by a compression wave, which occurs near the discontinuous change in wall curvature. For the small radius 2D nozzles used in this study, the same phenomena is also observed. The complicated expansion/compression waves were further analyzed by using the PLOT3D shock function, which computes pressure gradient multiplied by local Mach number (Figure 2.8).

2.4.4 Comparison With Test Data

In the turbojet nozzle throat, the expansion waves are followed by two compression waves, the stronger of which occurs on the upper throat wall due to the greater turning angle. The wave emanating from the lower throat wall has negative pressure gradient values (-1.3) which strike the upper turbojet wall which has pressure gradient values of (-2.4) due to the rapid area increase. Thus, as the lessor negative gradient expansion wave interacts with the wall, the pressure levels off, which is shown in Figure 2.9 at $0.4 < X/L9 < 0.6$. The expansion/compression-wave generated at the upper turbojet throat ($X/L9 = 0.23$) is also shown in Figure 2.9, where the CFD solution falls somewhat short of the test data at the maximum compression point. The turbojet lower cowl wall static pressure distributions (Figure 2.10) are not affected by the upper throat expansion/compression wave reflections, and are in good agreement with the test data. However, the expansion/compression wave generated on the turbojet upper throat, just downstream of the nozzle, does impact the shear layer just downstream of the confluence point. Waves reflect off of shear layers in the opposite sense, which would act to reinforce the compression waves at the confluence point, which is shown in the pressure gradient map (Figure 8).

The ramjet lower cowl wall static pressure distribution is shown in Figure 2.11. The expansion/compression wave from the ramjet lower throat wall reflects from the upper ramjet cowl wall, in like sense, with the surprising result, as a compression wave, which causes a slight increase in pressure on the wall at $0.14 < X/L9 < 0.18$ (Figure 2.11). The gradient value of this wave (Figure 2.8) is +.2, which accounts for the pressure rise. However, this wave is a combination expansion/compression wave, and when reflected, the expansion wave dominates and slows the pressure drop (Figure 2.12) on the wall at $X/L9 = 0.4$ as it is further reflected on the lower ramjet wall. The CFD static pressure is in good agreement with the data on all four walls of the configuration and shows the features of these waves which emanate from the nozzle throats.

2.4.5 Velocity Vectors in Turbojet Upper Throat

There was some speculation as to whether the flow was separated in the nozzle throats. The turbojet upper throat has the most severe turning, where velocity vectors in the throat flowfield show no reverse flow.

2.5 NOZZLE THRUST COEFFICIENT

The nozzle thrust coefficient was computed from the CFD solution using the following post processor formulation:

$$C_{fg} = \left[\sum_{\substack{\text{Exit} \\ \text{Plane}}} \frac{\dot{m}V}{g} + \left(P - P_{amb}\right) A \right] / F_{gi} \qquad (5)$$

$$F_{gi} = \dot{m}V_{ideal} = f\,(NPR, T_T) \qquad (6)$$

The NPR for the turbojet was 98.288 and 67.961 for the ramjet. The ambient pressure was 60.9 psf, T_T turbojet = 5.28.8 R T_T ramjet = 528.51 R and Tamb = 520 R.

For this two nozzle case, the dividing streamline was determined from the streamline map (Figure 2.7) and two thrust coefficients computed. These two coefficients were then mass averaged for a value of 0.985 compared with the experimental value of 0.979. The 3-D CFG value computed later on was 0.9807, which is in better agreement with the experimental value.

2.6 CONCLUDING REMARKS

(1) Several convergence criteria were met including the massflow convergence in both nozzles. CFD mass flow was computed both in the nozzle throat and confluence point plane and when these became equal and steady (as a function of interation number) the convergence criteria was met.

(2) The shock behavior at the confluence point represent some loss in total pressure and angularity coefficient and can be predicted by CFD and reasonably well by inviscid theory, where viscous effects are small.

(3) Small radii nozzle throats cause the flow to expand rapidly just downstream of the throat, where the high angular momentum must be reduced to meet the tangential wall boundary condition. This must be accomplished by a compression shock. These expansion/ compression waves interact with the walls causing pressure anomalies.

(4) The experimental nozzle is almost perfectly expanded to ambient pressure which allows the CFD downstream extrapolation boundary condition to be valid in its application.

(5) The CFD pressure gradient contour map is extremely valuable in interpreting flowfield phenomena.

(6) CFD wall pressures are in good agreement with data on all four walls. This test data indicates that the expansion/compression waves generated in the nozzle throat region are combinations of these two types of waves, with one or the other dominating.

(7) From Figure 2.7, it is observed that the two jets will not be well mixed. Similar conclusion will be made in the Phase -3 study of ejector flow in the turbine-based - combined - cycle propulsion system.

(8) The results of this research had been published in the 30th AIAA/ASME/SAE/ASEE Joint Conference in 1994 (Reference 11).

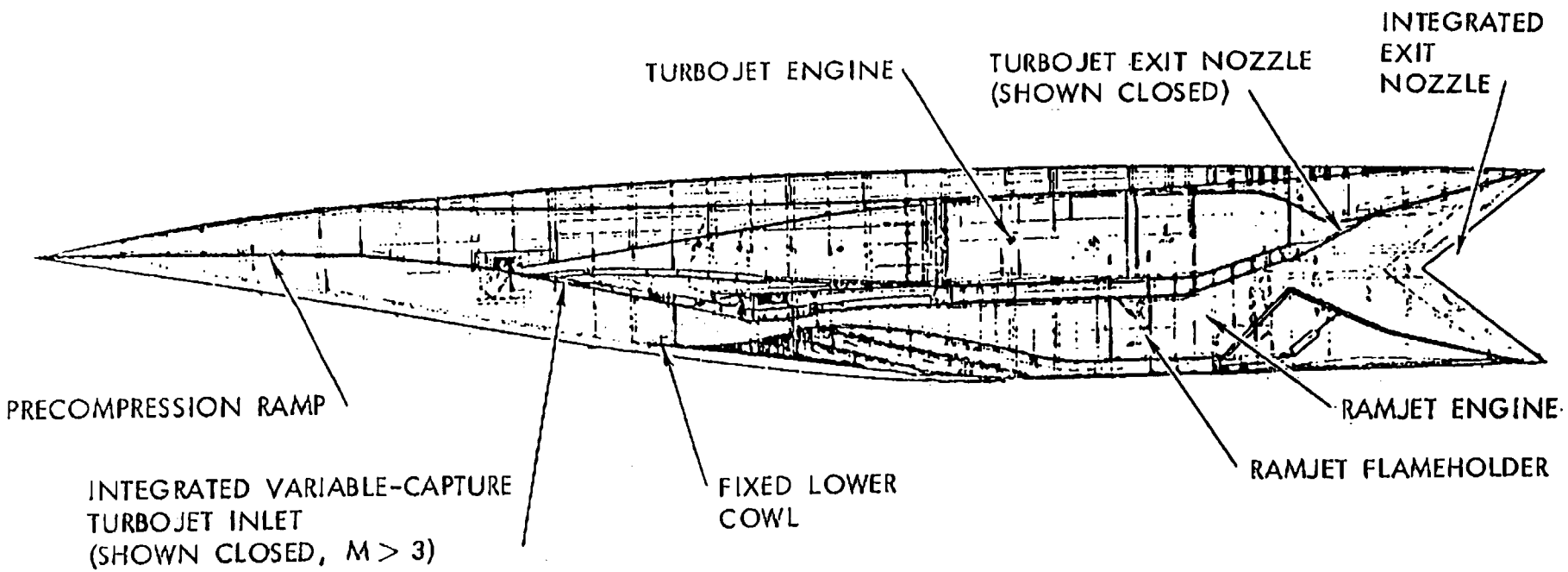

Figure 2.1 Typical Over/Under Turbojet-Ramjet Configuration

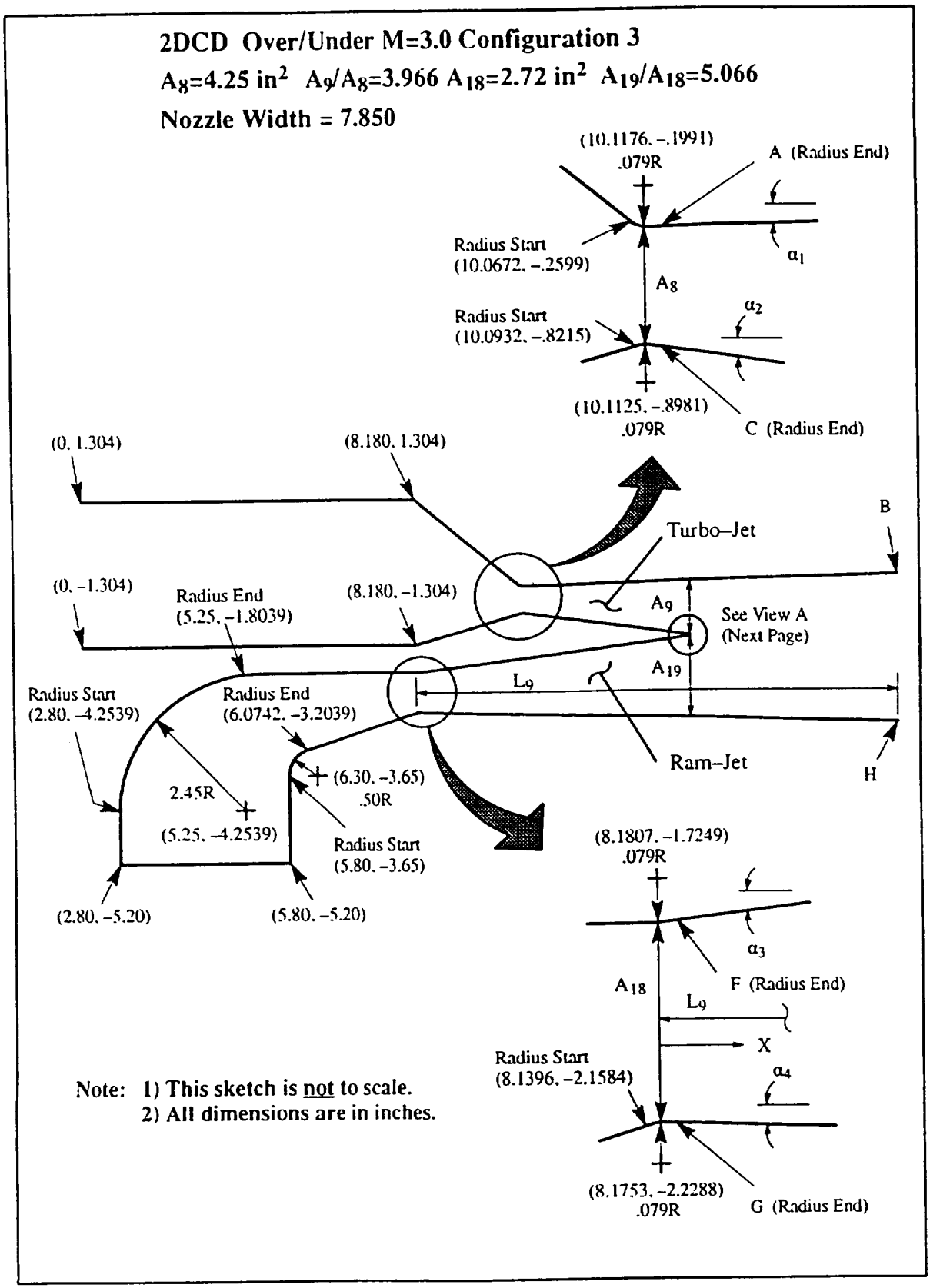

Figure 2.2 2DCD Over/Under M = 3.0 Configuration

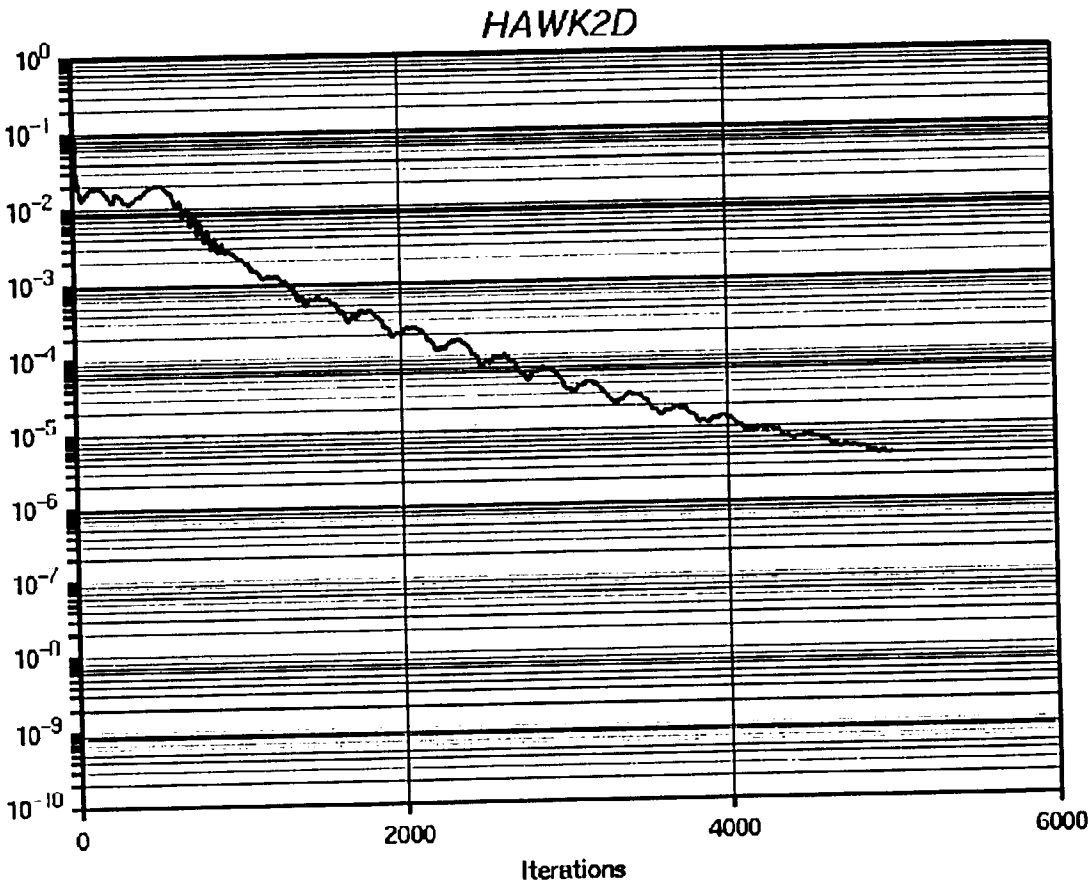

Figure 2.3 L2 Residual Drops Six Orders of Magnitude in 5000 Iterations

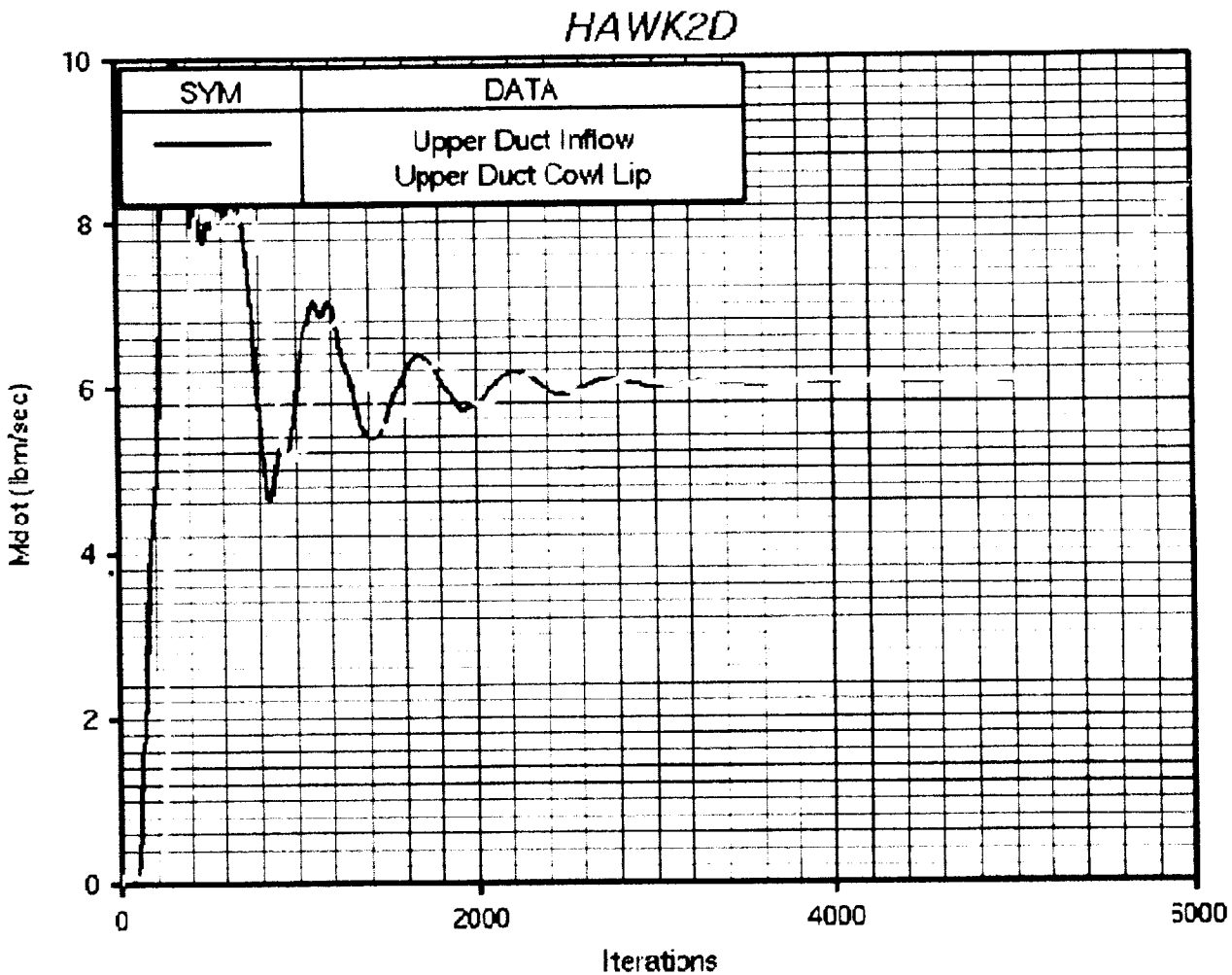

Figure 2.4 Turbojet Mass Flow (Per Unit Width) As a Function of Solution Iterations

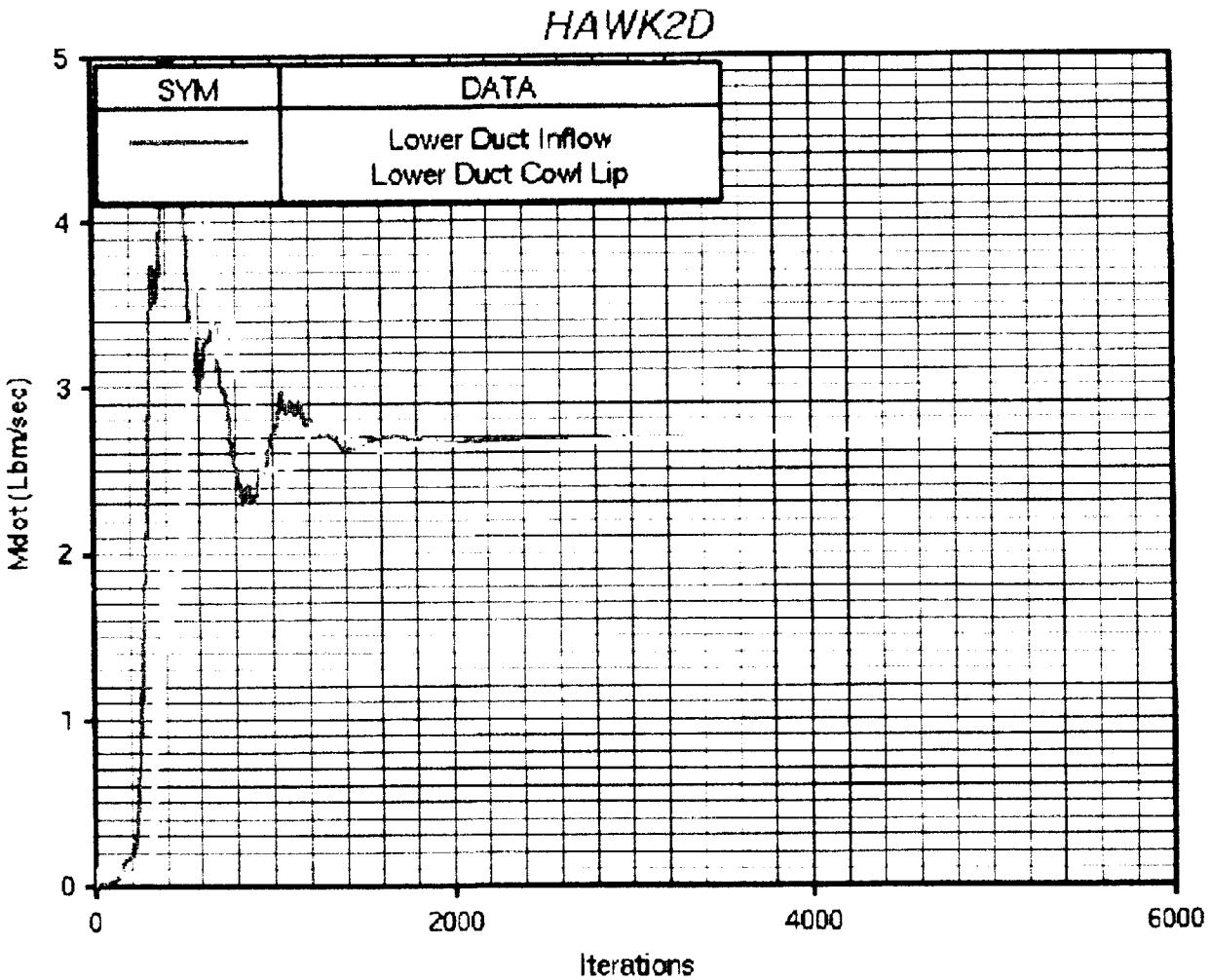

Figure 2.5 Ramjet Mass Flow (Per Unit Width) As a Function of Solution Iterations

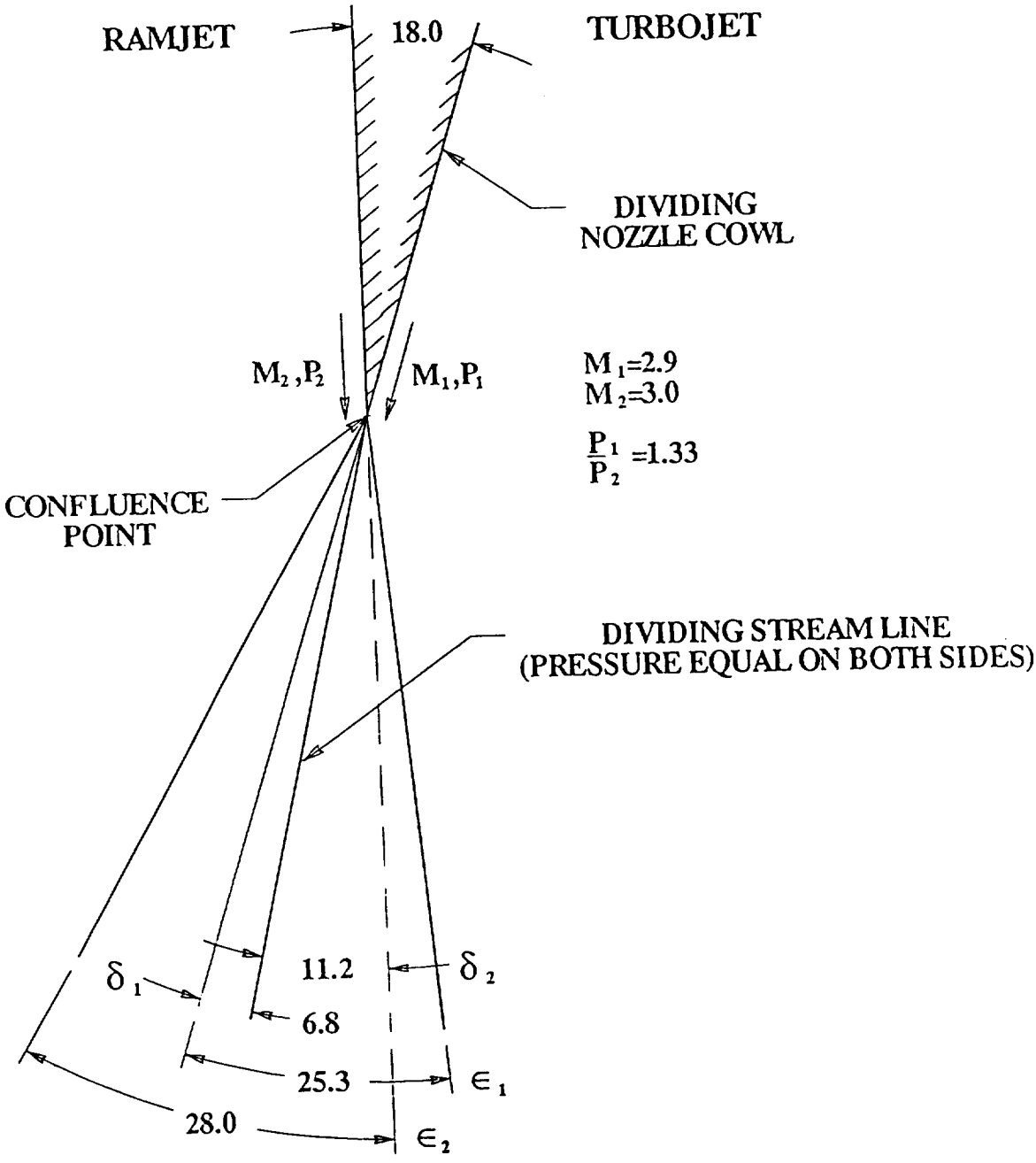

Figure 2.6 Inviscid Relationships at Confluence Plane

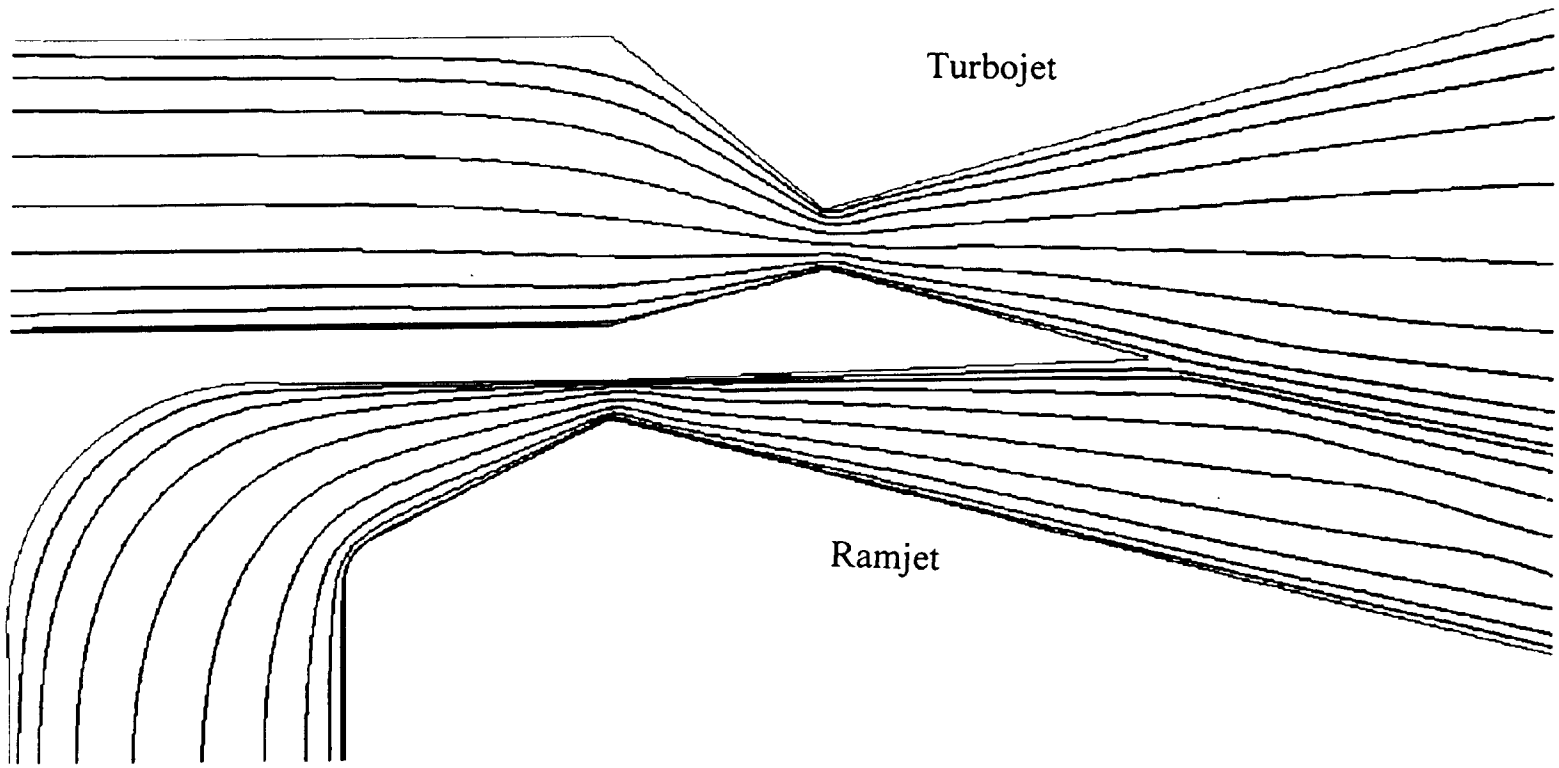

Figure 2.7 Turbojet and Ramjet Streamlines

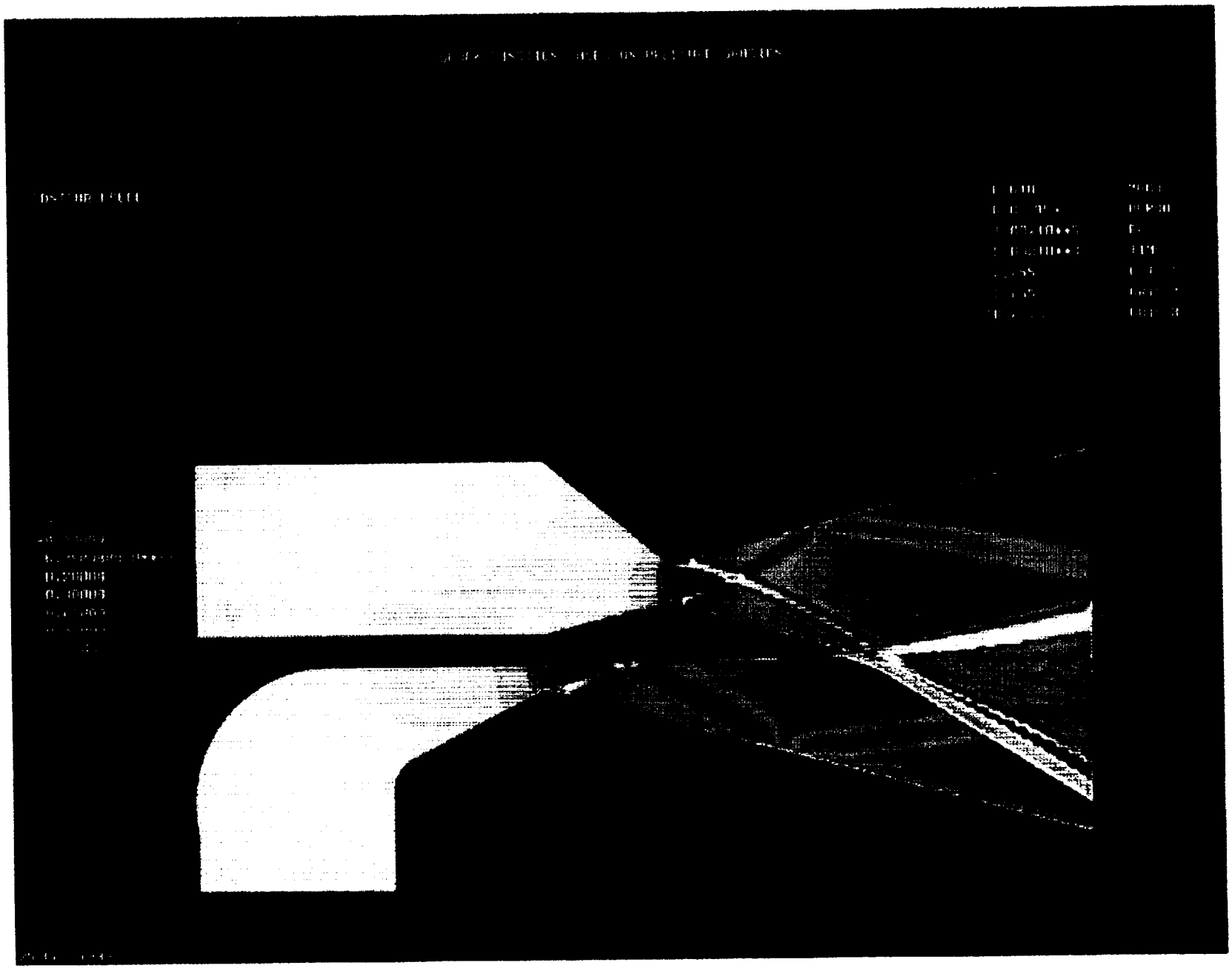

Figure 2.8 Pressure Gradient Contour Map of Over/Under Nozzle Flowfield

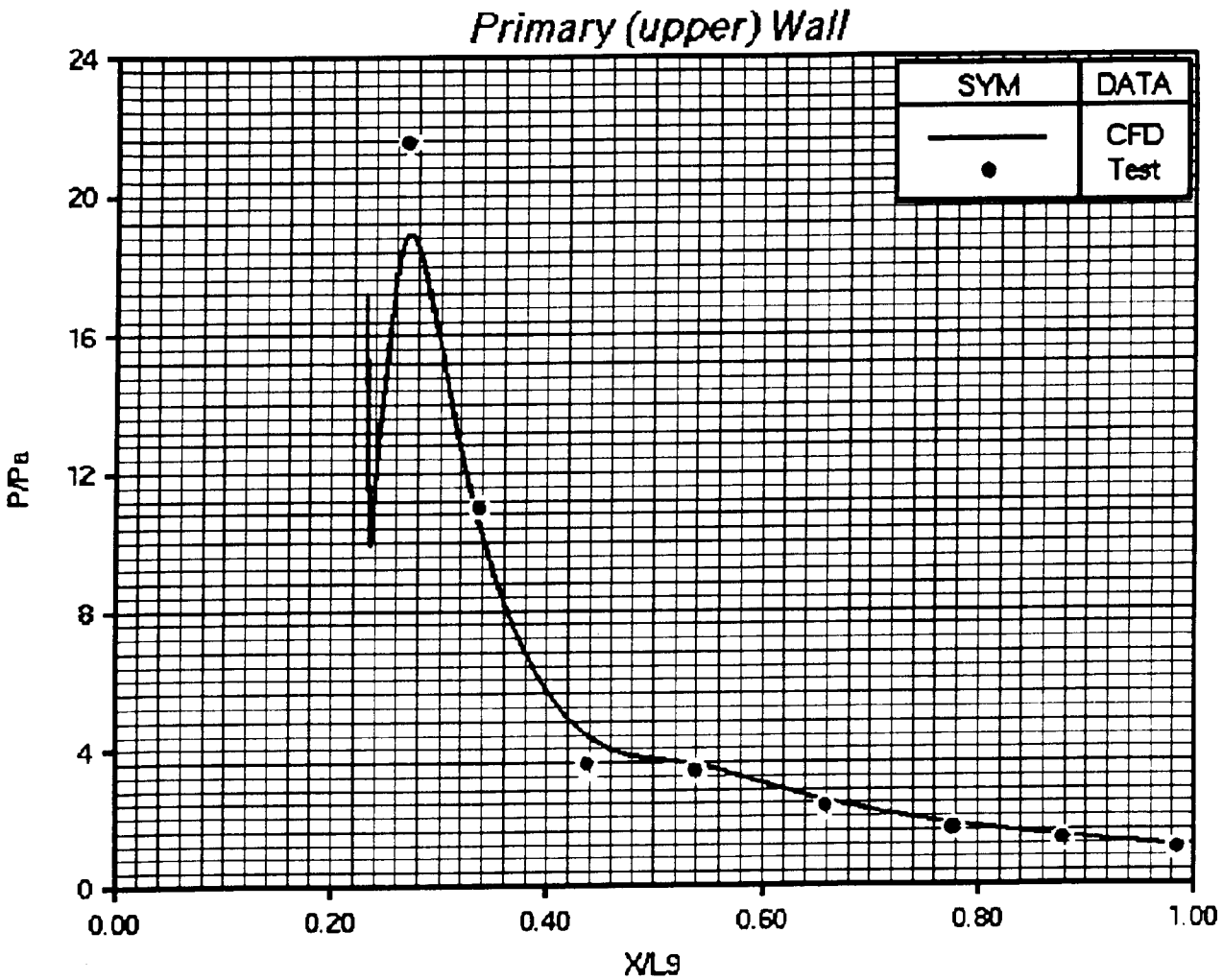

Figure 2.9 Turbojet Upper Wall CFD Pressure Distribution with Data

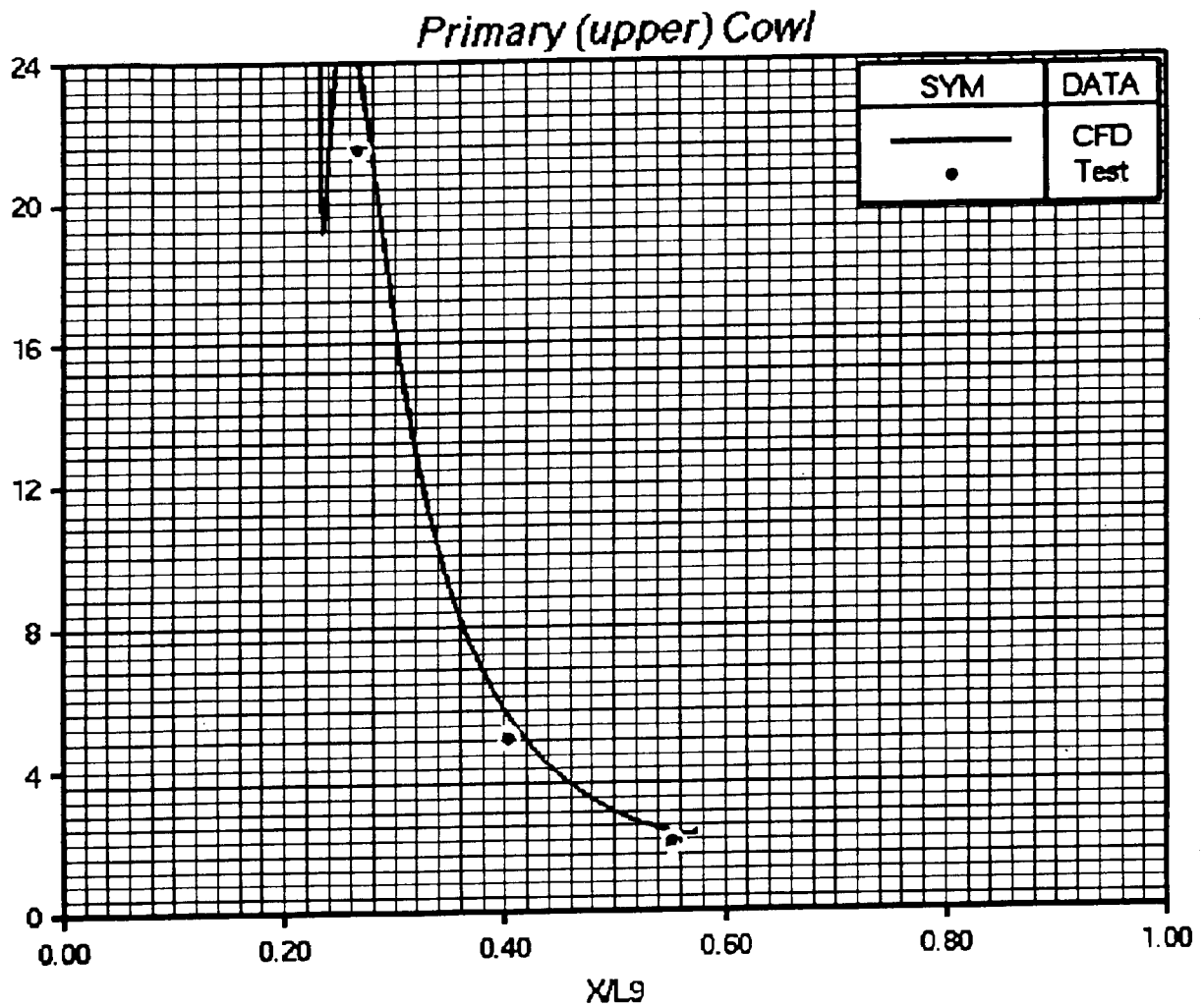

Figure 2.10 Turbojet Lower Wall (Cowl) CFD Pressure Distribution with Data

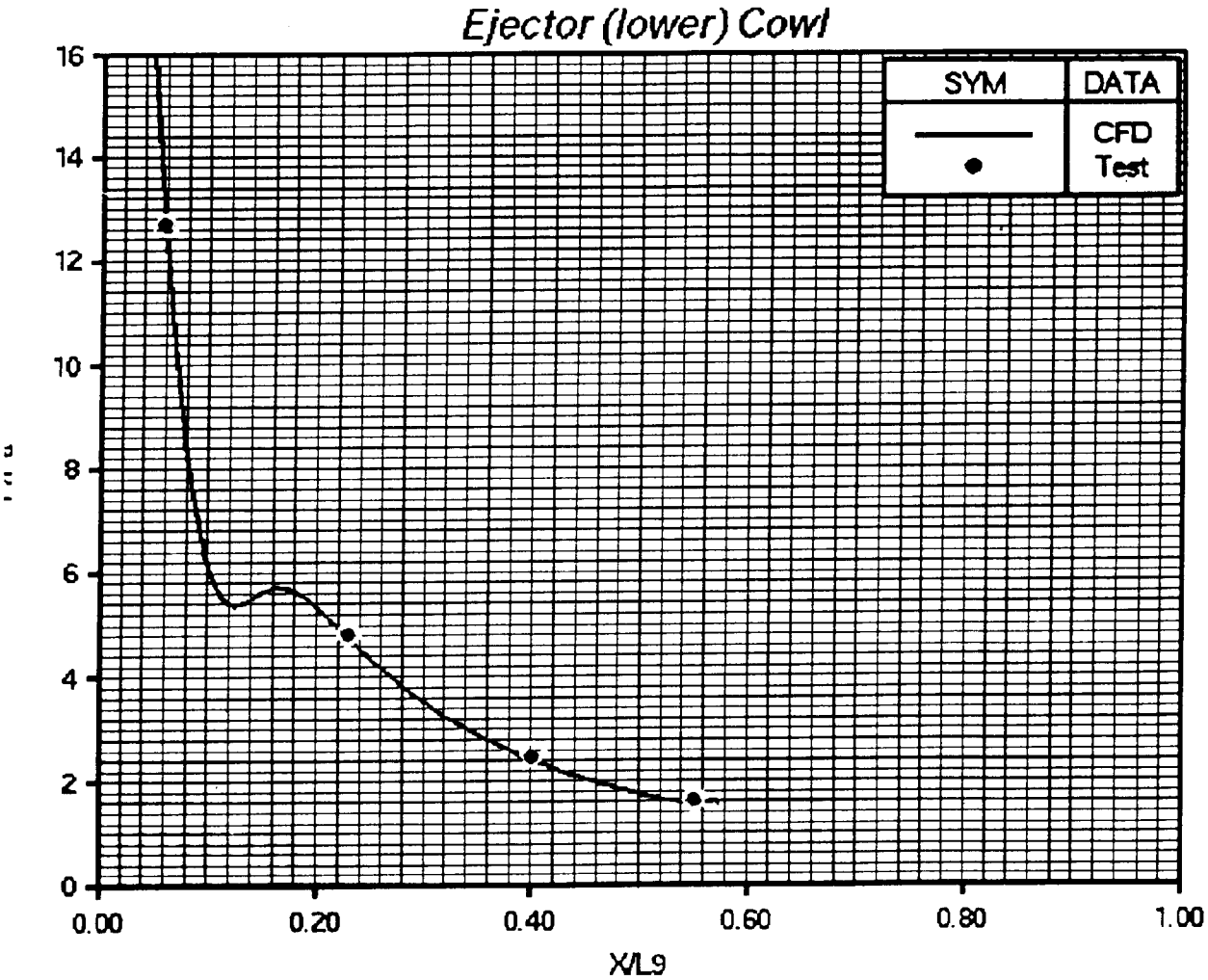

Figure 2.11 Ramjet Upper Wall (Cowl) CFD Pressure Distribution with Data

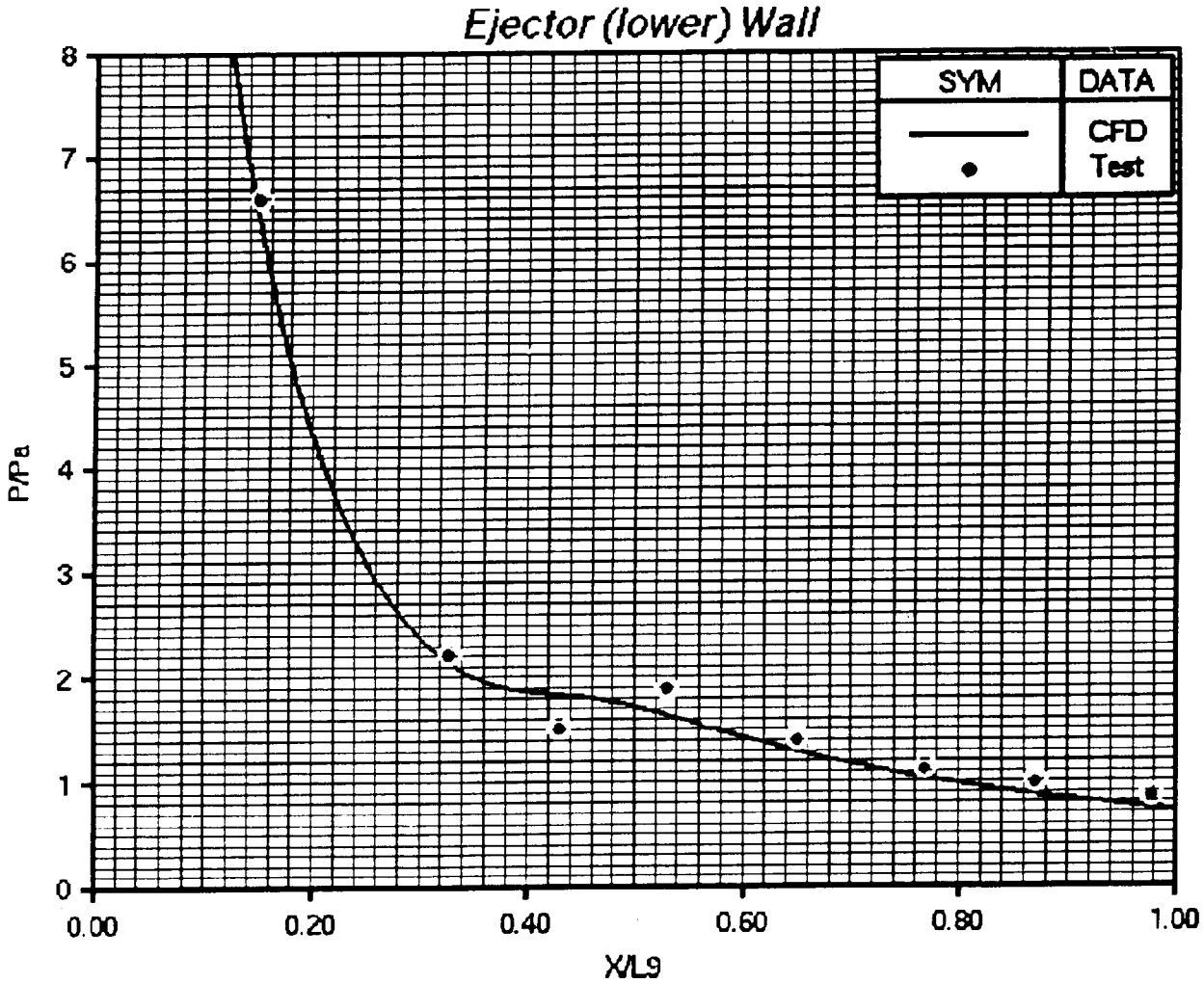

Figure 2.12 Ramjet Lower Wall CFD Pressure Distribution with Data

3. Over/Under Nozzle CFD Study - Three Dimensional Analysis

3.1 INTRODUCTORY REMARKS

The test data supplied from NASA/Lewis Center for CFD solution comparisons were from a model with a nozzle width of 7.850 inches. The cross sections of the nozzle are rectangles. At the ramjet throat, the width to height ratio is 22.7, and at the turbojet throat, the ratio is 14.5. At the confluence of the two jets (the cowl tip), the width to height ratio is 2.0, and at the common nozzle exit, the ratio is 1.34. So, as a first approximation, it is reasonable to assume the nozzle flow is two dimensional. That analysis has been discussed in the last chapter. But for a more accurate comparison, especially in the region between the cowl tip and the exit of the nozzle, It is desirable to extend the study to 3-D configuration. This is the second phase of the research and will be discussed in this chapter.

3.2 CONFIGURATION

The grid for 3-D case was 232 in the axial direction and 170 in the normal direction with 22 planes in the tranverse direction. Because of symmetry, the plane at the centerline is treated as a symmetry boundary condition and numbered k = 22, where the sidewall is numbered as k = 1. The grid distribution at I = 232 (the exit of the common nozzle) is shown in Figure 3.1 as well as the initial planes at I = 1. The confluence point is at I = 121. A typical grid distribution is shown in Figure 3.2, which is at I = 130. In this figure, there are more grids closed to the walls as well as the vicinity of shock interactions. The location of shock interactions were obtained from 2-D analysis. The grids were generated by GRIDGEN3D code.

3.3 CFD SOLUTIONS

The flow solver used for the CFD analysis is a NPARC3D code with k-k1 two equation turbulence model (HAWK code). The 3-D code had run 5000 iterations, the residual as a function of iterations was plotted in Figure 3.3, which indicates the mass flow rate in the ramjet (blue) essentially converged and the turbojet (red) almost converged. Shown in Figure 3.4 is a density distribution on a transverse cross section at I = 200. The figure shows thin boundary layers on the walls, a thin shear layer between two jets, and nearly uniform transverse density distribution. A longitudinal Mach number distribution at k = 10 is shown in Figure 3.5, higher Mach number in the upper half of the common nozzle is observed. Shown in Figure 3.6 is a 3-D longitudinal and transverse composite Mach contour plot. The transverse cross section shown is at I = 232, noticed the symmetry to the mid-longitudinal plane at K = 22. The short longitudinal plane is due to the almost normal projection on the transverse plane. Figure 3.7 and Figure 3.8 are density contour maps. They show greater property variation longitudinally, also sharper shocklines when the flow is closer to the centerline. Figure 3.7 is at k = 20, and Figure 3.8 is at k = 10. The measured centerline pressure data compare very well with CFD results, where the transverse pressure distributions are seen to drop slightly as the outer wall is reached (Figure 3.9). The most notable result is the streamline patterns on the wall. The 3-D CFD results show the streamlines near the wall going down the shock line instead of the deflection angle experienced by streamlines away from the wall (Figure 3.10, 3.11). This 3-D phenomena is referred to as glancing shock-interactions on inlet and nozzle sidewalls. In inlet flowfields, the glancing shocks are more aggravated because of the inlet and adverse pressure gradient. The nozzle does experience some adverse pressure gradients because of the over-expansions at the nozzle throats. However the pressure gradients are still dominantly very favorable. The Mach 5

inlet test run at NASA/Lewis showed the flow migration down the inlet shocks to have a major influence on inlet performance. The vertical flow migration in inlets can break loose from the wall, thus avoiding bleed, and enter the high speed inlet causing inlet/engine compatibility problems (Reference 12 to 17).

3.4 CONCLUDING REMARKS

(1) Static pressures are lowered as the wall is approached.

(2) The glancing sidewall shock interactions entrain flow from the boundary layer down the shockline, distorting the flow near the sidewall. The same phenomena is found in inlets.

(3) The gross thrust coefficient (CFG), thrust divided by ideal thrust, is lowered from 0.9850 (2-D) to 0.9807 (3-D), where the experimental value is 0.9790. The glancing sidewall shock could account for some of the reduced CFD value.

(4) From the 3-D CFD analysis, it shows the earlier 2-D CFD analysis is a very good approximation.

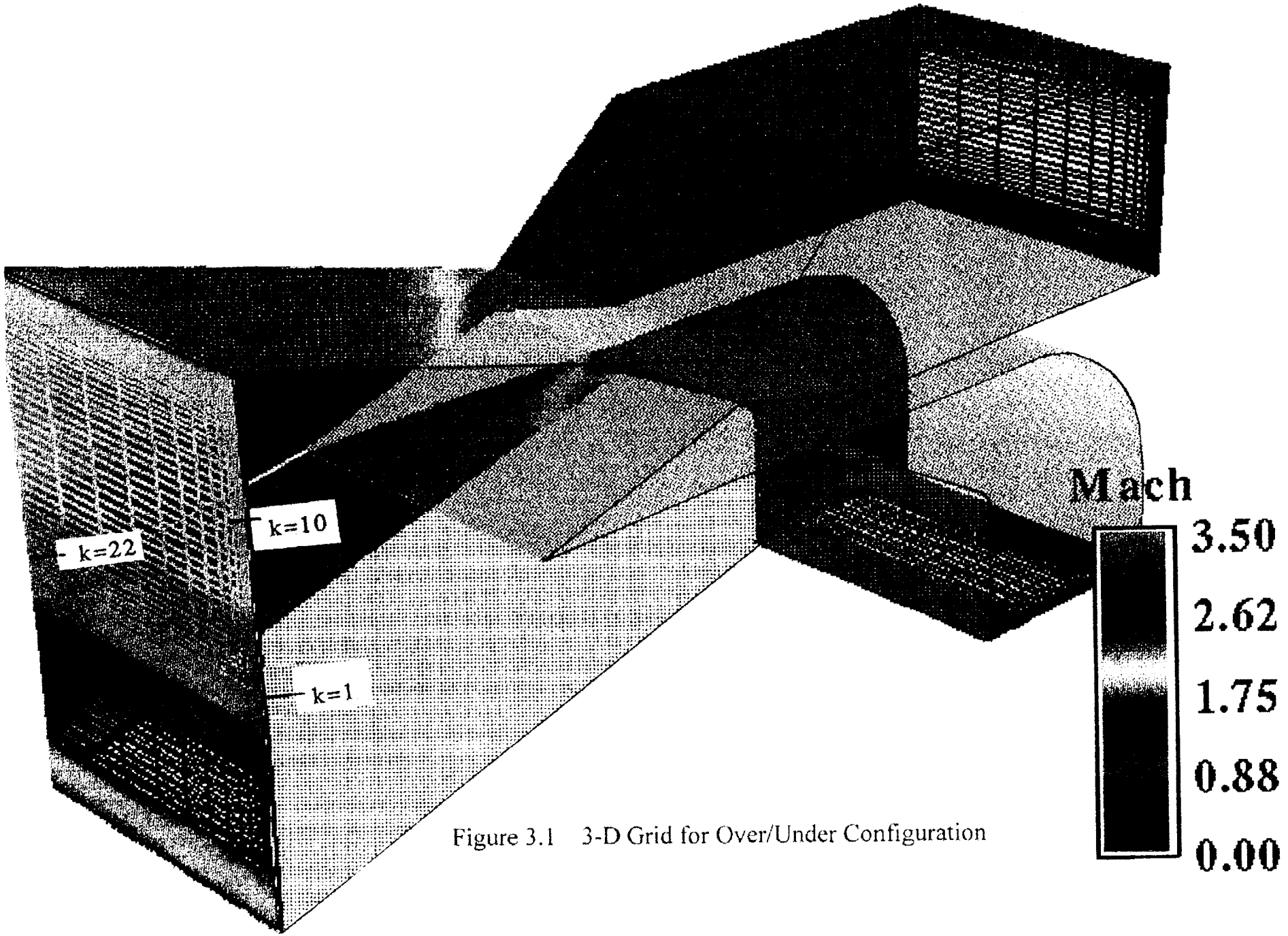

Figure 3.1 3-D Grid for Over/Under Configuration

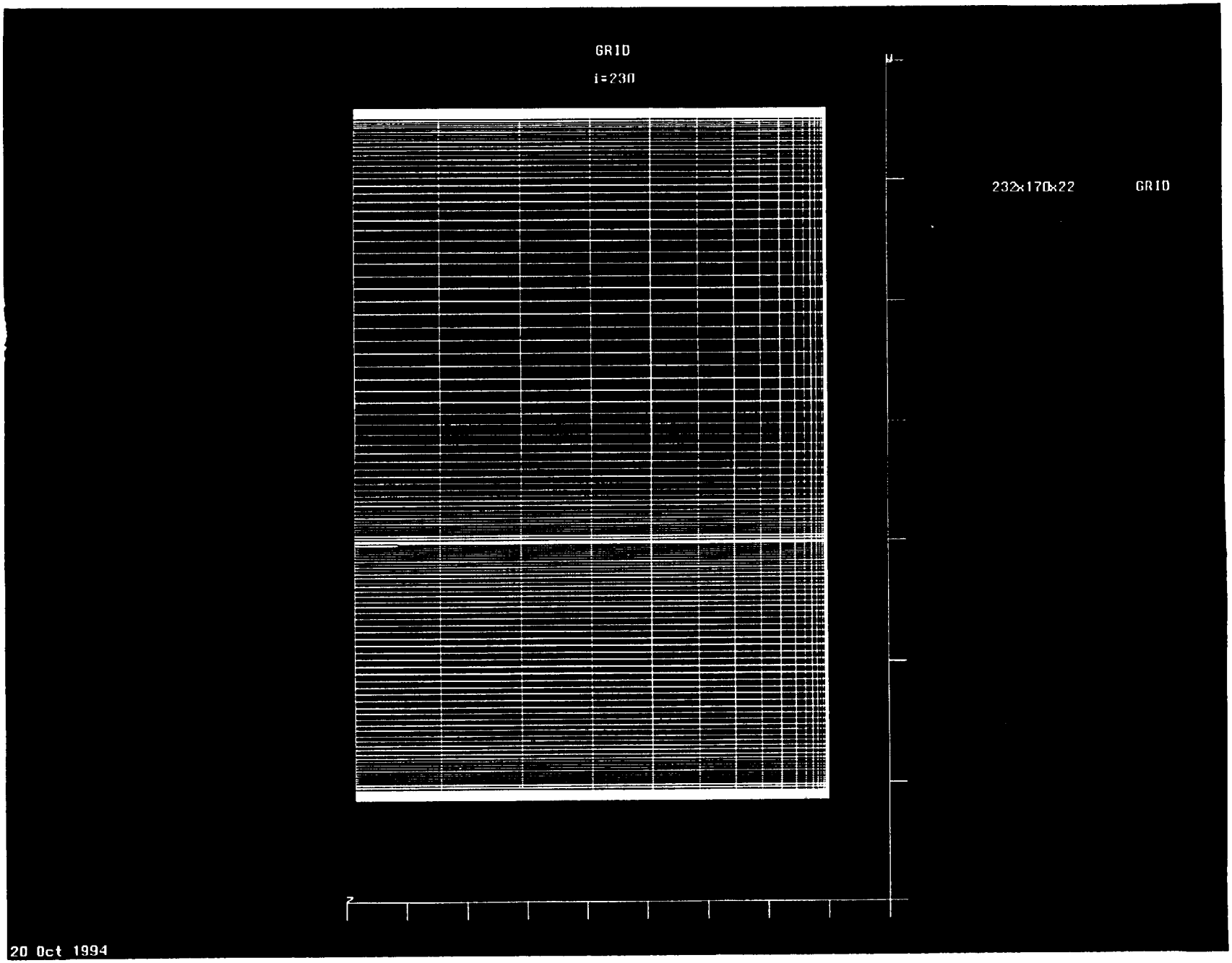

Figure 3.2 Grid Distribution at i = 230

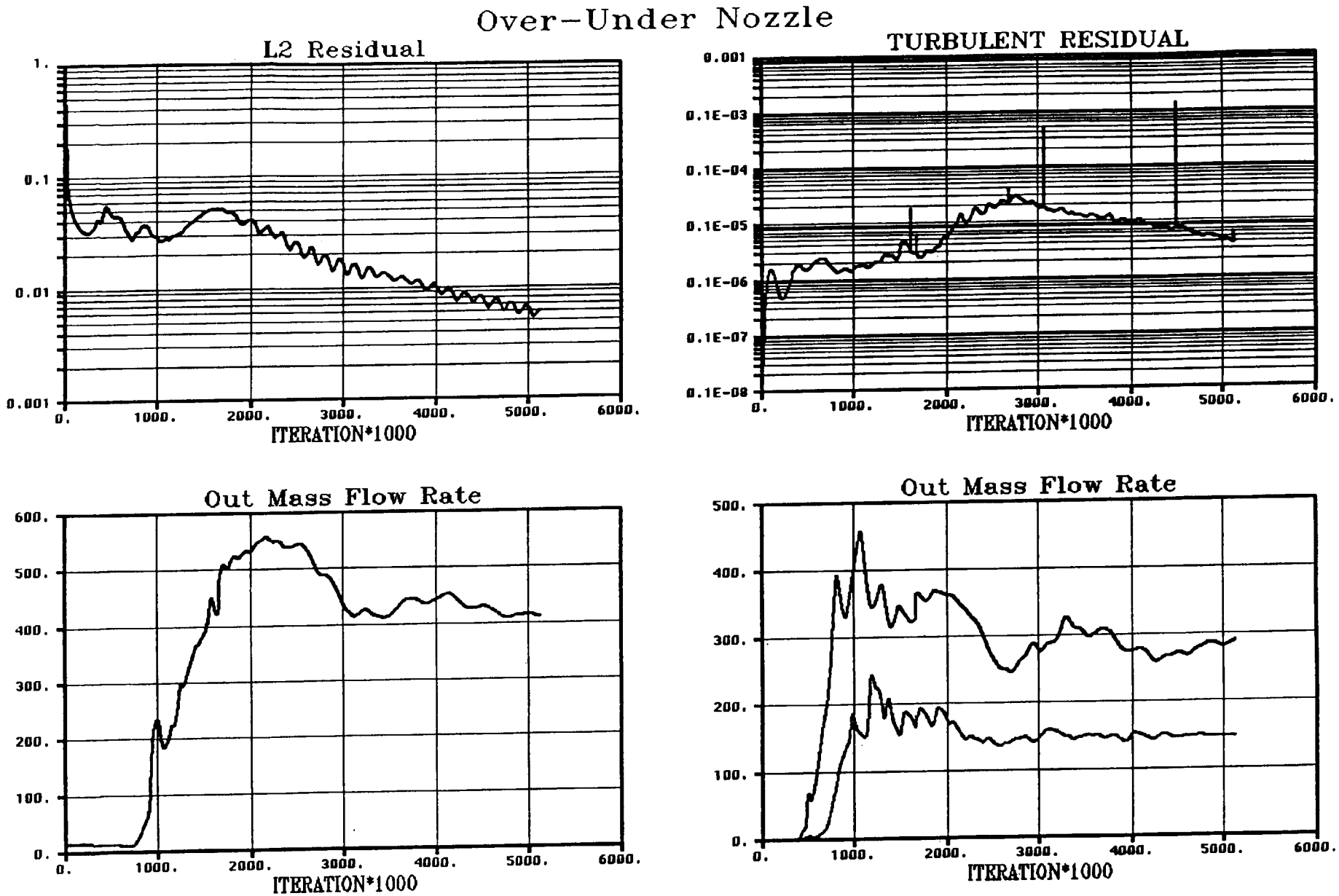

Figure 3.3 L2 Residual,Turbulent Residual, Mass Flow as a Function of Iteration

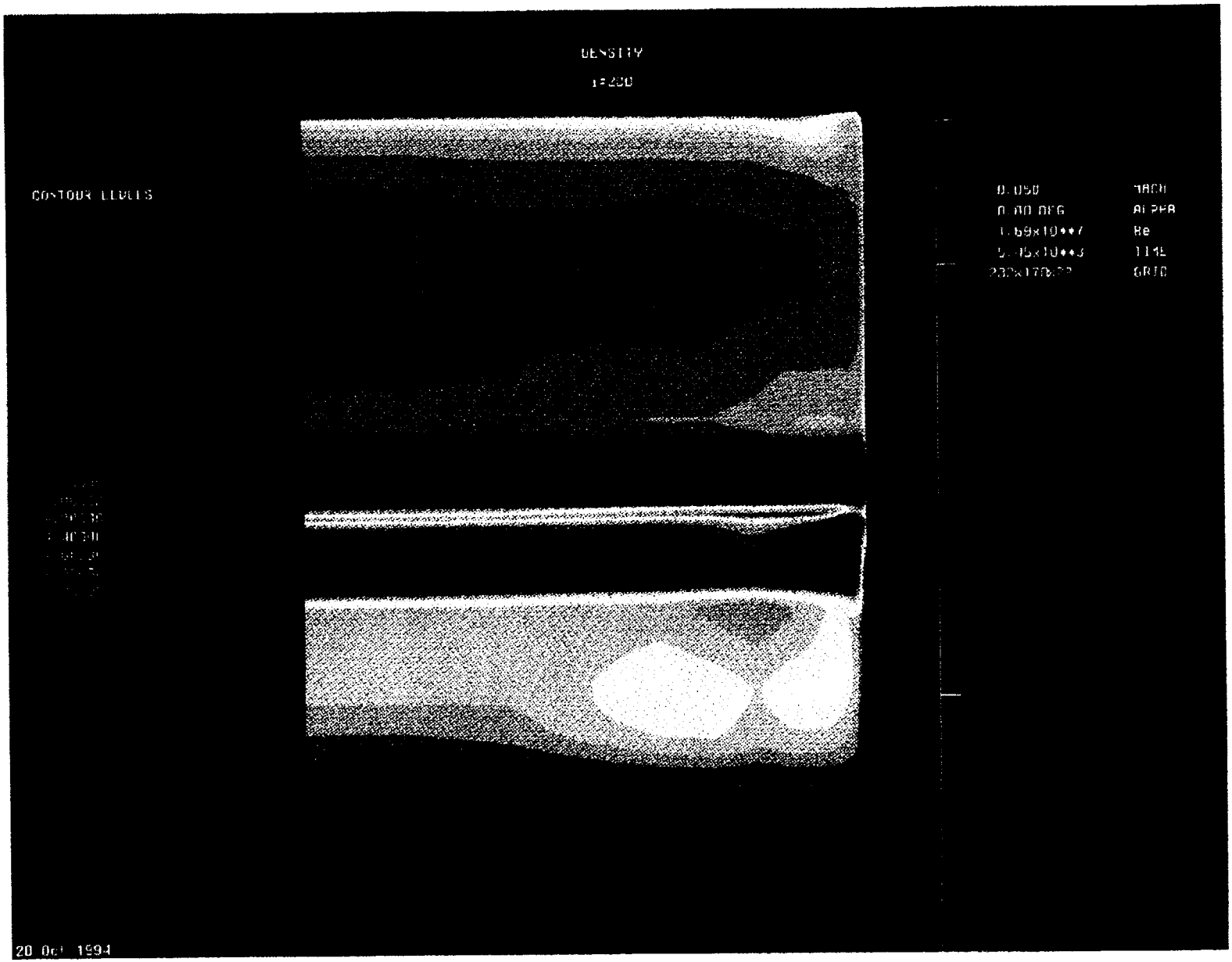

Figure 3.4 Density Distribution at i = 200

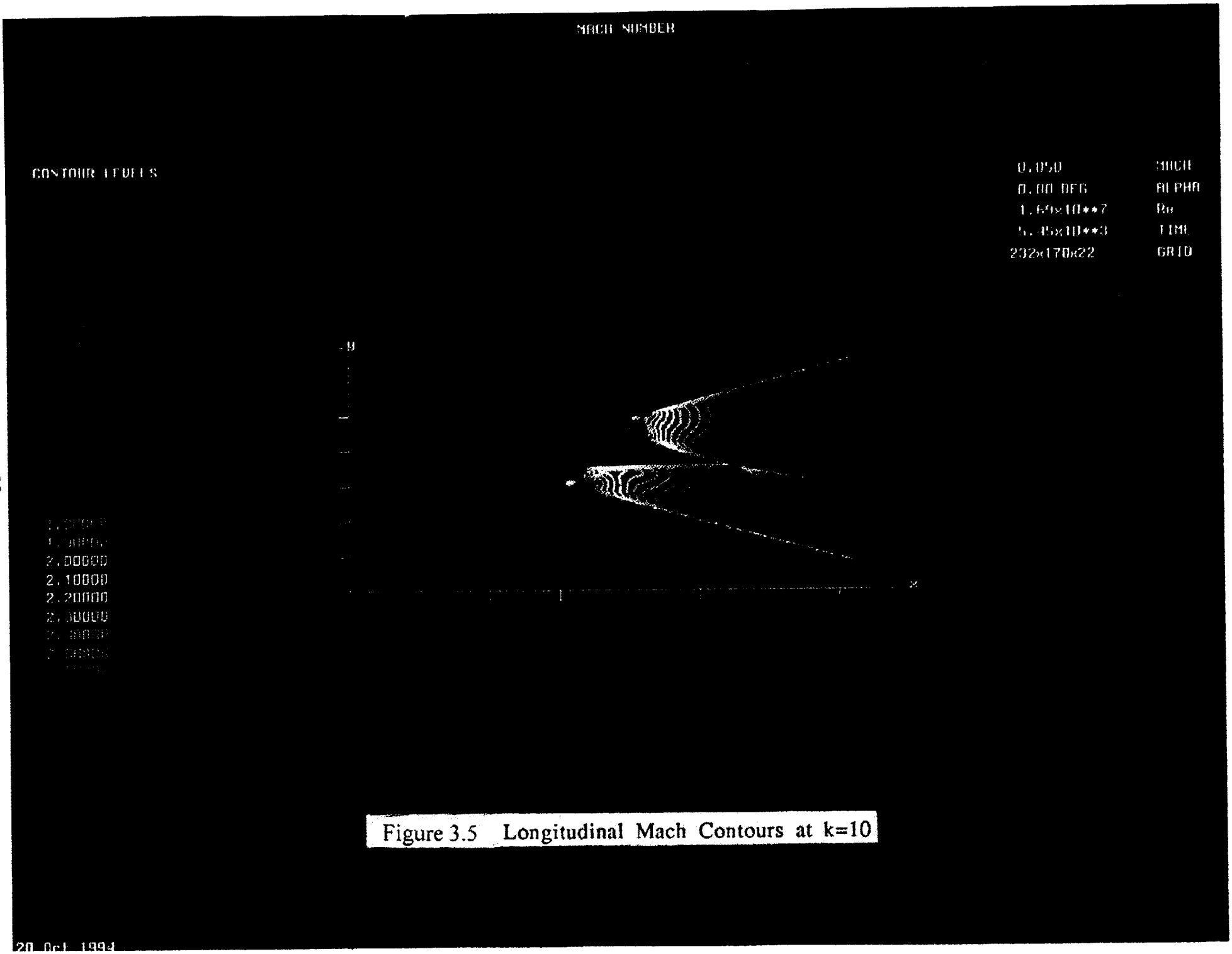

Figure 3.5 Longitudinal Mach Contours at k=10

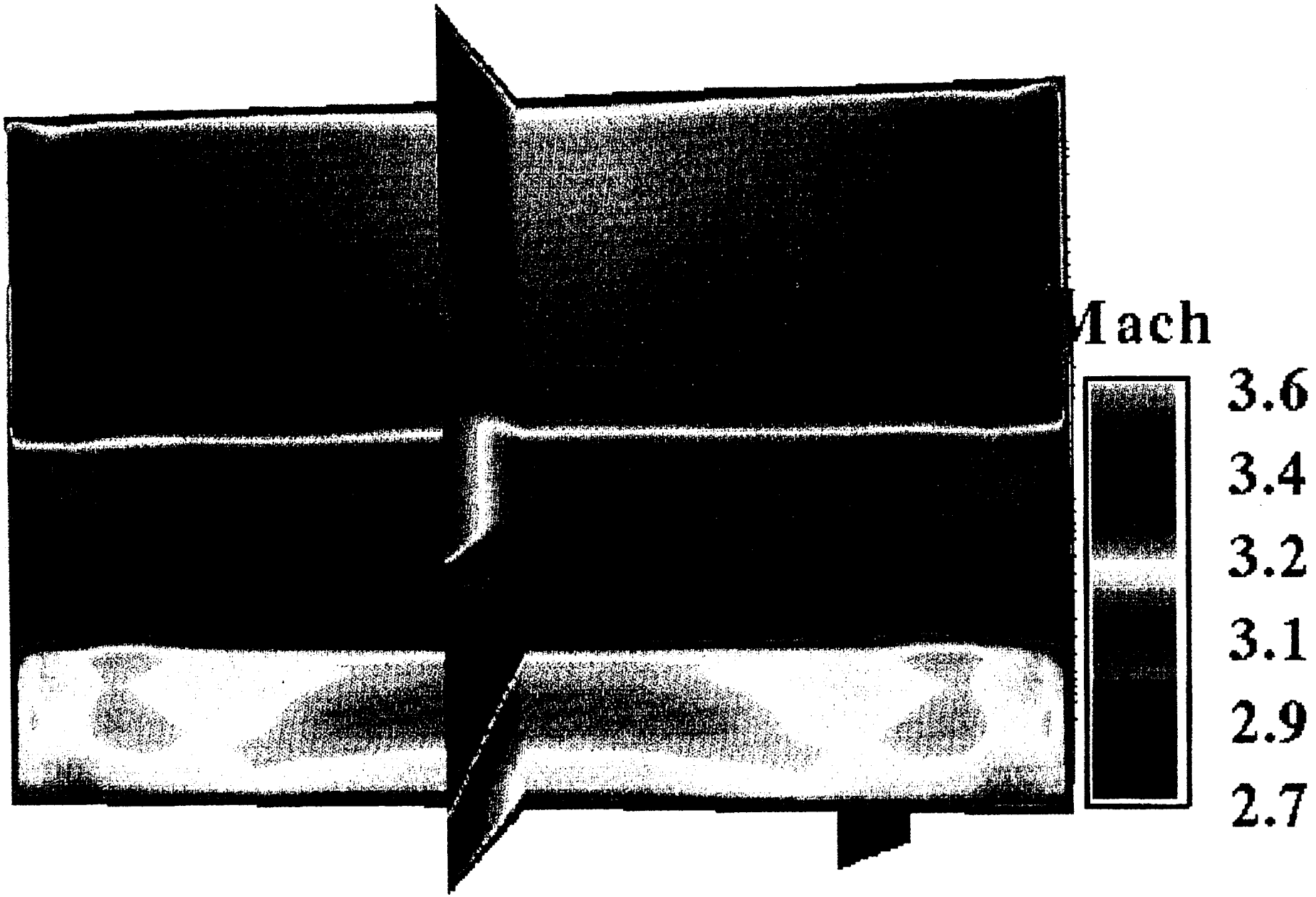

Figure 3.6 Mach Contours Showing Transverse and Longitudinal Distribution

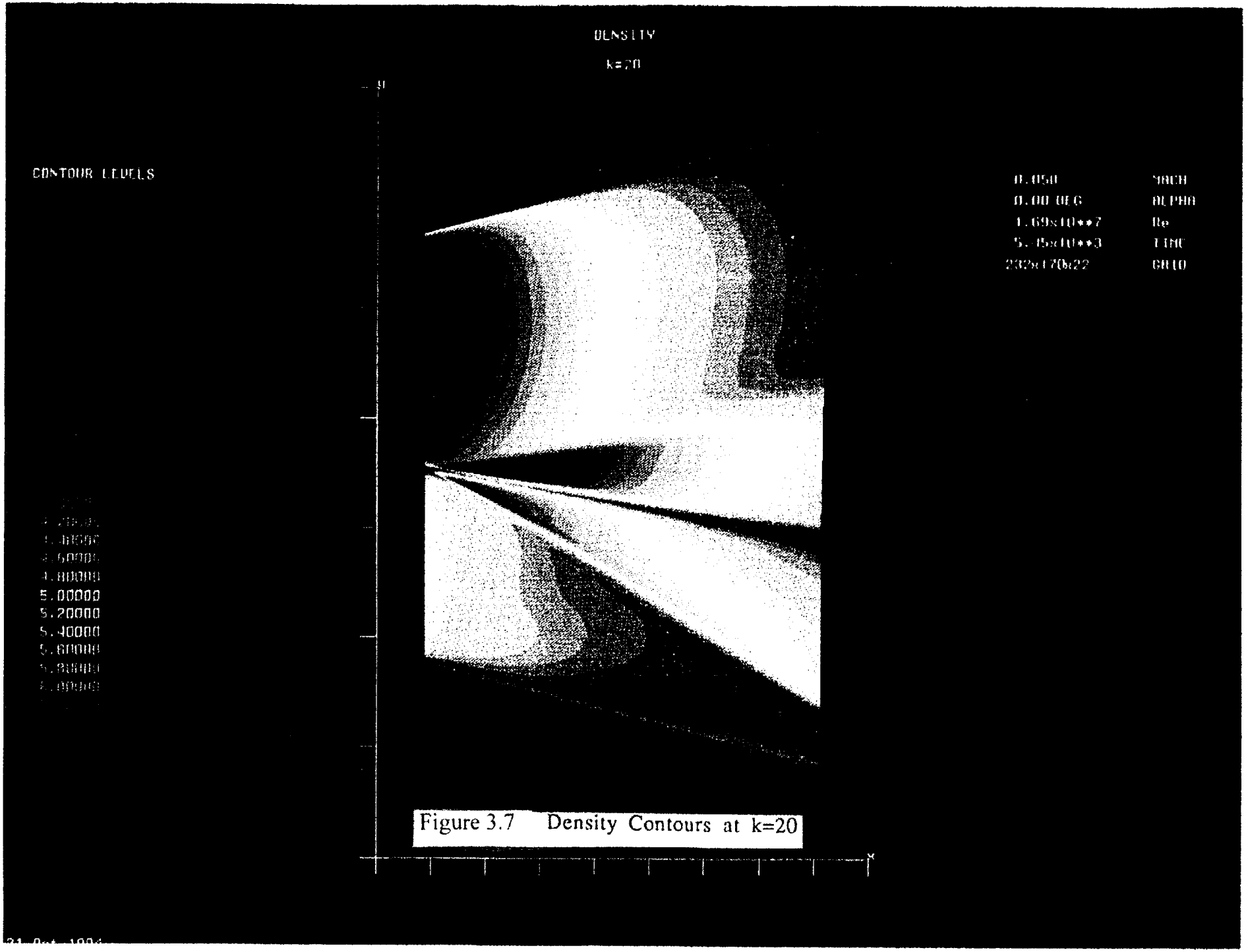

Figure 3.7 Density Contours at k=20

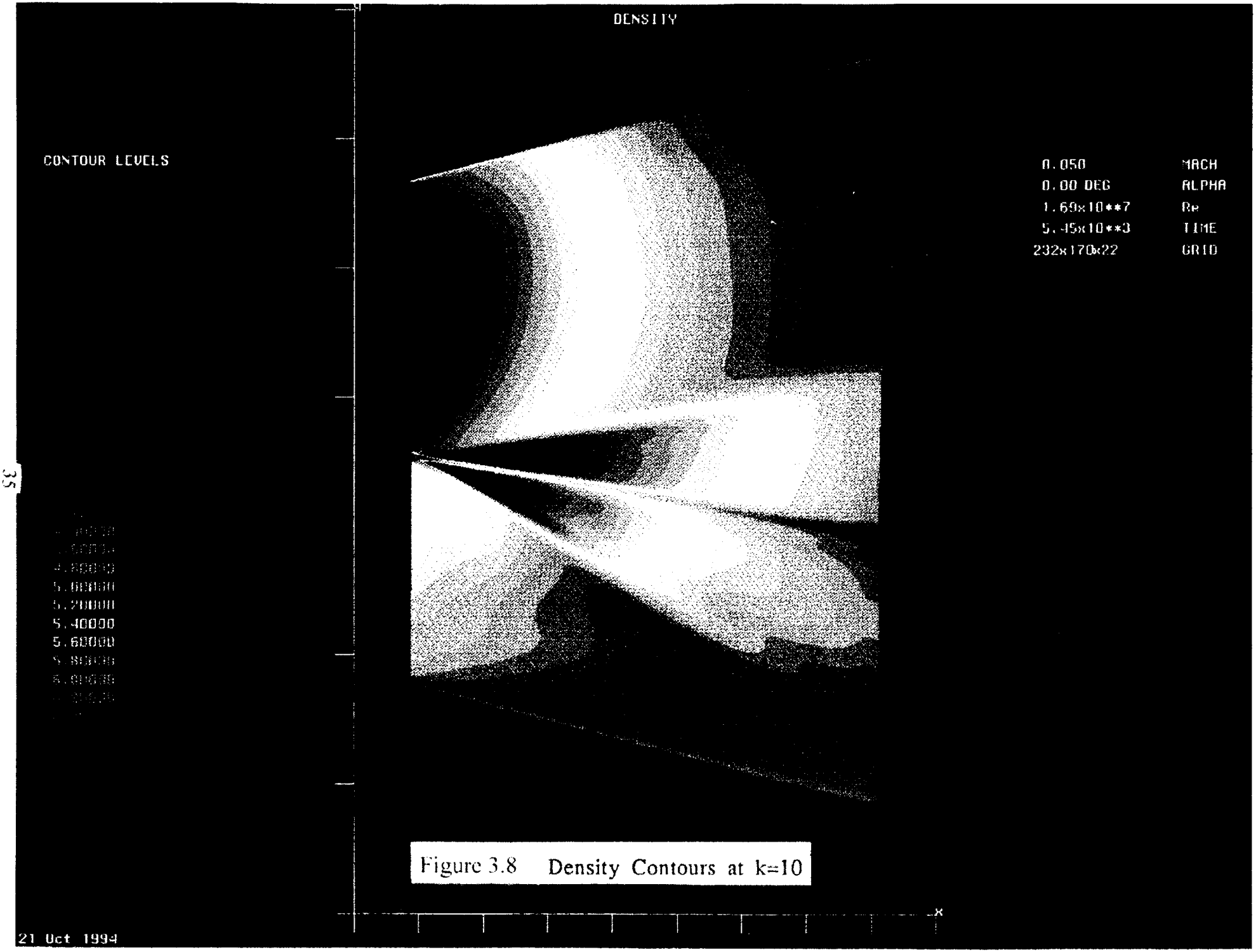

Figure 3.8 Density Contours at k=10

Over/Under Nozzle (U)

Surface Pressures (Pa=60.9 psf)

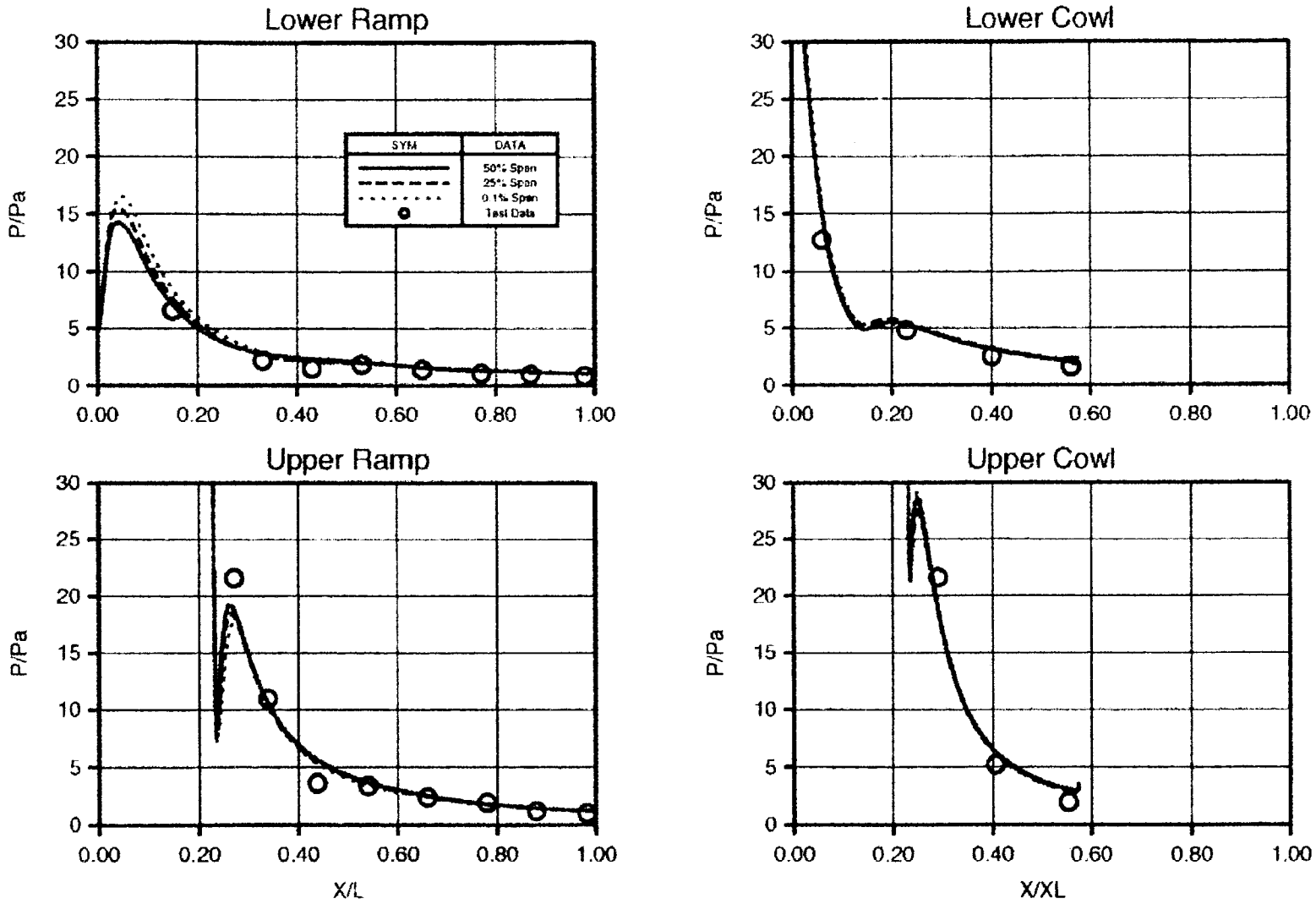

Figure 3.9 Surface Pressures on Lower and Upper Cowls and Ramps

TJW
18-Oct-94

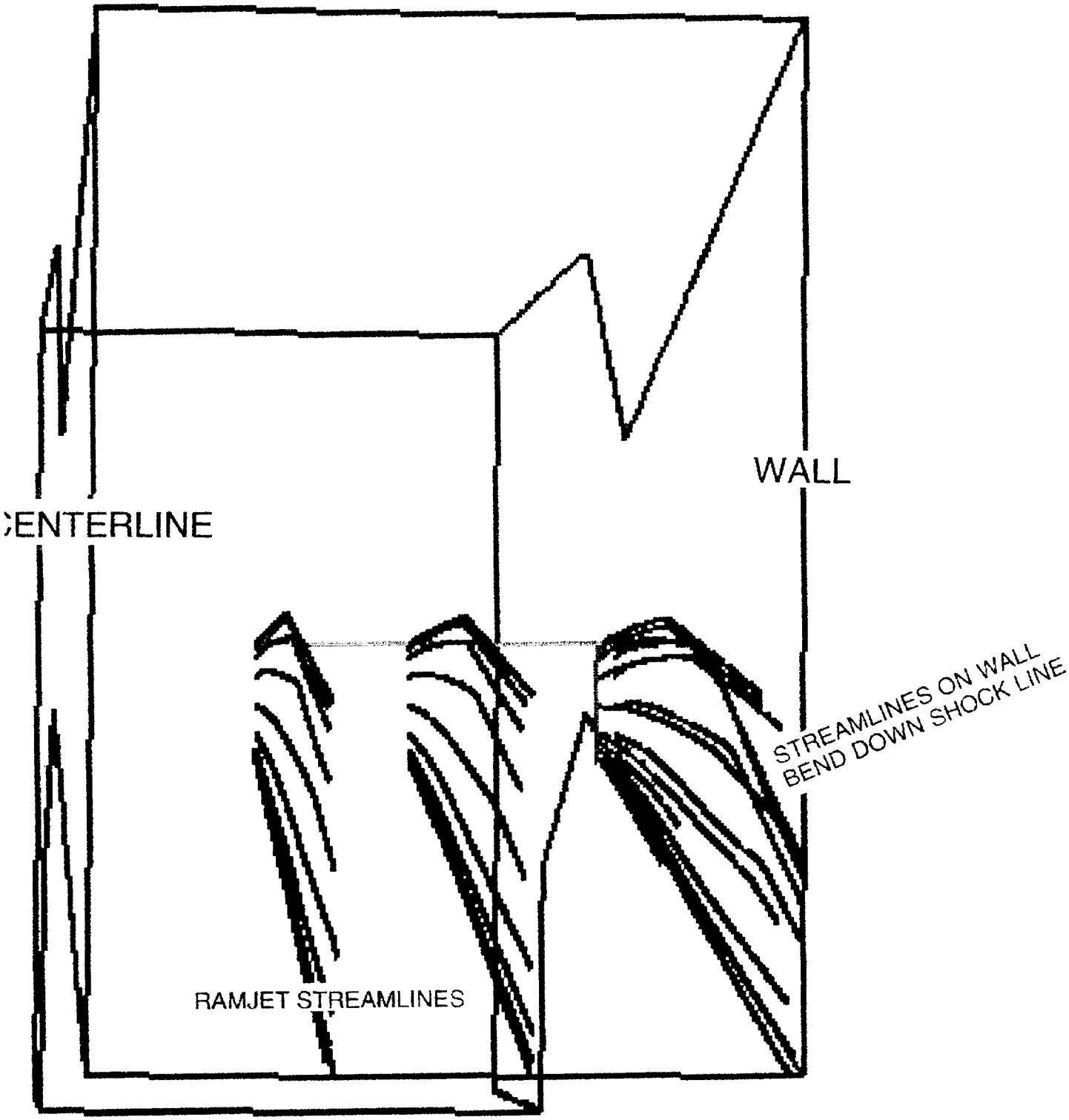

Figure 3.10 Streamlines Released at the Wall and Inboard Streamlines for Comparison

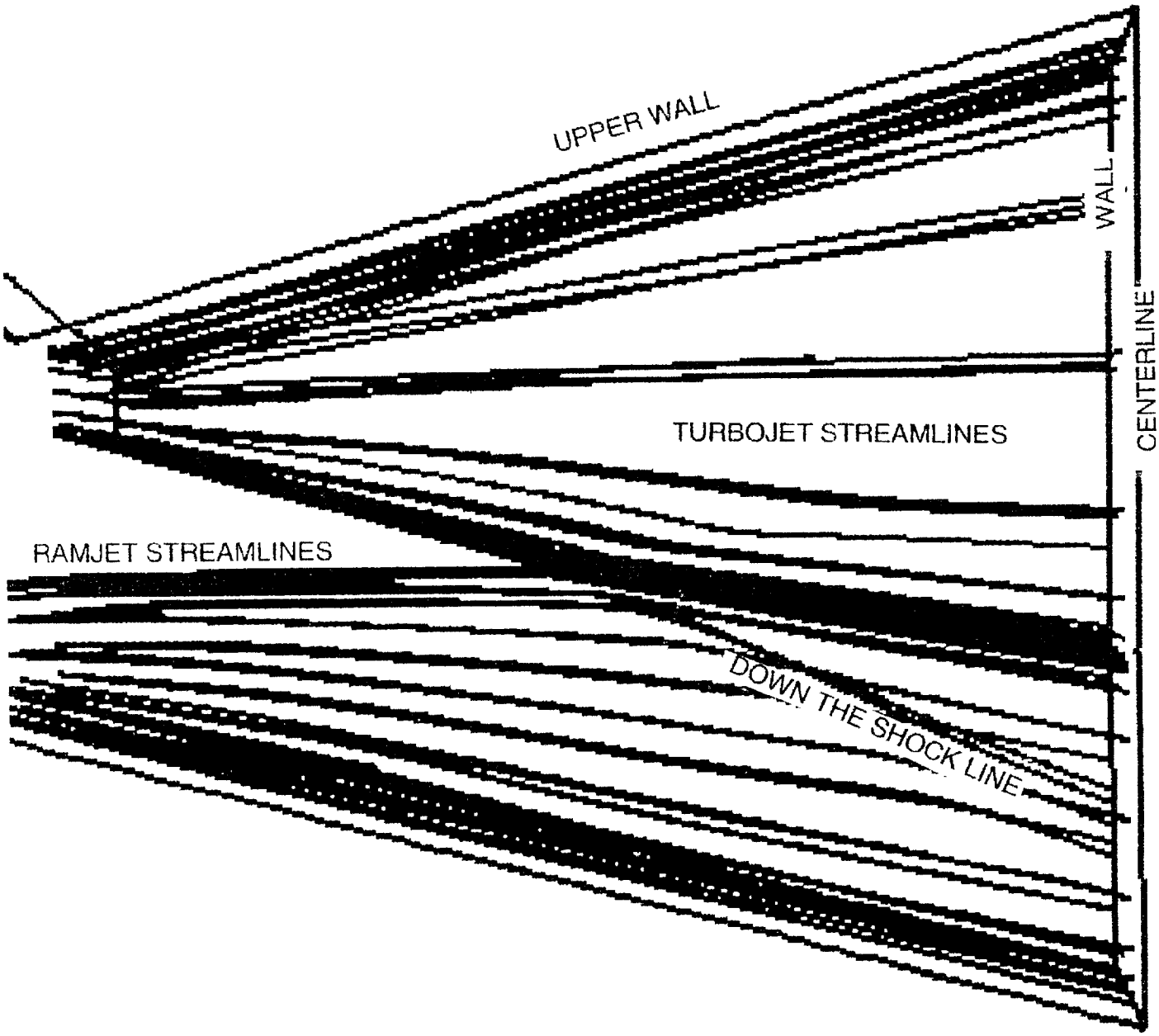

Figure 3.11 Streamlines Flowing Down Shockline on Outer Wall

4. Supersonic Ejector Turbojet/Ramjet Propulsion System

4.1 INTRODUCTORY REMARKS

In this phase of study, a different turbo-ramjet configuration was analyzed. Specifically, the confluence of a supersonic turbojet and a subsonic ramjet in the turbine-based-combined-cycle (TBCC) propulsion system was studied by a 2-D CFD code.

Supersonic ejector-diffuser systems have application in driving advanced airbreathing propulsion systems, consisting of turbojet engines acting as a primary stream and a single throat ramjet acting as the secondary stream. The turbojet engines are integrated into the single throat ramjet to minimize variable geometry and eliminate redundant propulsion components. The result is a simple lightweight system that is operable from takeoff to high Mach numbers. At certain high Mach number (approximately Mach 3.0), the turbojets are turned off and the high speed ramjet/scramjet systems take over and drive the vehicle to Mach 6. The turobjet-ejector-ramjet system consists of nonafterburning turbojet engines with ducting canted at approximately 20 degrees to the ramjet ducting. The turbojet ducting goes through a C-D nozzle causing the flow to expand to approximately Mach 1.4 when it mixes with the subsonic ramjet secondary flow. This flow interacts, in ejector mode, with the secondary ramjet acting at total conditions prescribed by the inlet recovery conditions (Reference 18). If the secondary flow chokes in the mixing zone, maximum flow is obtained in the ramjet duct, which is a major component of thrust. This condition is known as the Fabri choke condition. As the downstream backpressure is increased, the Fabri condition can no longer exist and the ramjet is reduced and the ejector is no longer back pressure independent. However, a high backpressure near critical ejector conditions represents the maximum thrust which can be obtained by the system. Therefore these

conditions are the ones which are the major concern of this study. Two cases will be studied, one where the ejector is critical and one where the back pressure is sufficient to cause the ejector to go slightly subcritical. Other ejector geometries were evaluated as to their capability to effect maximum secondary flow.

4.2 COMPUTATIONAL TOOLS

The simplified analysis in supersonic ejector flow is the 1-D control volume analysis. Constant area and constant pressure assumptions had been made in the analysis of Addy, et al (Reference 19). The TBCC analysis used the constant area assumptions for their ejector analysis and had incorporated this segment into a comprehensive propulsion deck capable of total propulsion integration into a system study vehicle. Trefny and Benson of NASA/Lewis Research center had developed a TBCC 1-D Code for their analysis (Reference 20). In order to determine the second order effects, a 2-D Navier-Stokes code was used to study this ejector system in our research. The code of choice was the FALCON - kkL finite volume procedure (Reference 21). The k-kL turbulence model is a two-equation formulation mentioned earlier (Reference 4). The results will be compared with 1-D TBCC results.

4.3 CONFIGURATION

A schematic diagram to show the features of TBCC propulsion system is given in Figure 4.1. Notice that the ejector region is approximated with a constant area duct. As mentioned before, two cases were studied here. The free stream conditions were Pinf = 627 psf and Tinf = 413R, the Mach number = 2.0. The turbojet total conditions were Pt = 5935 psf and Tt = 1815 R. After expansion through a nozzle, the Mach number of the turbojet enters the ejector region is approximately 1.4. The secondary total conditions for the ramjet stream were Pt = 3882 psf and

Tt = 732 R. The secondary mass flow (or Mach number) is not specified, it is part of the solutions.

The secondary height is 10.92 in. and the primary height is 10.89 in. The mixed region height is 15.29. Ratio of specific heat is assumed to be 1.4, but can be changed to be a function of local temperature. Wall conditions were assumed to be slip, but in the 2-D CFD study, the turbulence model was activated for all interior points, which includes the primary/secondary mixing zone. A typical 1-D TBCC results for these conditions are shown in Figure 4.2, the outputs in figure can be changed readily through active interaction with the computer. The 1-D TBCC results will be used to compare with 2-D CFD results.

For the 2-D analysis, the confluence point at the entrance of the ejector region is modeled by multiple grid points, with approximately 30 points upstream of the confluence point for both the primary and secondary sides. To avoid the computation of thermal choke due to heat addition, it is replaced by a computational choke to supply the back pressure. There are 229 x 109 grids generated by the GRIDGEN2D code. More grids were given around inlets and the mixing region of the two jets (Figure 4.3).

4.4 CFD SOLUTIONS

4.4.1 Boundary Conditions

For the HAWK flow solver, the boundary conditions are applied at cell faces (the region between grid points). There are 17 boundary condition types in the flow solver. Applied to the ejector region, at the ramjet inflow, specified the total pressure and total temperature. At the turbojet inflow, fixed boundary conditions are given. At the supersonic flow behind the

computational throat, characteristic farfield supersonic outflow condition is assumed. At the wall surface, slip surface condition is assumed.

4.4.2 The Supercritical - Fabri Choke Case

This is the case that secondary ramjet choked in the mixing zone. The Mach number contour plots are shown in Figure 4.4. The primary nozzle entrance conditions are Mach 1.4, and immediately shock down to approximately Mach 0.8. A shock is formed around the confluence point due to high pressure secondary which interacts with the supersonic primary, where the pressures are considerable lower (Figure 4.5). The secondary flow does not mix substantially in the first few feet of the ejector, necks down and chokes at approximately 4.8 ft. The choked secondary location is known as the breakpoint or Fabri choke location. This flow represents the maximum flow for a fixed primary/secondary total conditions. The maximum secondary flowrate is 27.4 pps, where the primary flow is 63 pps. This is compared with the TBCC results, which shows the TBCC results to be 38 pps. The temperature contours are shown in Figure 4.6, from this figure, it should be noted that the primary flow and secondary flow are not well mixed. The upper and lower wall pressures are shown in Figure 4.7, upper and lower wall temperatures in Figure 4.8, and the Mach number in the secondary flow in Figure 4.9 (very close to wall at j = 30). This case has a slight area change as seen in the figures, and therefore deviates from the constant area 1-D model. Later cases will be given for constant area CFD formulations.

4.4.3 The Non-Critical Case

This is the case of Non-Fabri on Non-Break-Point condition. Since the back pressure is supplied by a computational choke. By varying the area of the nozzle, back pressure may be varied. Figuer 4.10 shows the CFD choke area to be decreased, which drives the ejector from critical to

non-critical. Figure 4.11 shows the normalized pressure contours as well as the converged averaged conditions across the primary, secondary and mixed conditions. The flow rate at the secondary drops slightly. Figure 4.12 shows the Mach number contour map along with the specified boundary conditions. The upper and lower wall pressure solutions are shown in Figure 4.13 and temperature contours in Figure 4.14, which again show the two flows are not well mixed.

4.4.4 Critical-Constant Area Case

Figure 4.15 shows a approximately constant area configuration with contoured walls in the primary to tailor the geometry for a more invigorated supersonic flow in the primary as was suggested by Addy. The primary and secondary areas are essentially equal, as it was in the two cases studied above. This tailored geometry allows more secondary flow to be injested thus increasing the vehicle thrust. Figure 4.16 shows the Mach number contours and boundary conditions. The pressure plots are shown in Figure 4.17. This flowrate is more in line with what the TBCC code predicts.

4.5 CONCLUDING REMARKS

(1) Near constant area results are in closer agreement with TBCC results.

(2) By area tailoring, the supersonic flow can be made to persist over a longer region and allows more secondary flow to be injected.

(3) Wall pressure distributions can be produced for any geometry, which will assist in future non-constant area/constant pressure cases by allowing for a thrust term to be included.

(4) Mixing of the two streams will probably require some physical devices.

(5) The computational throat needs to be replaced by a thermal choke in the future CFD analysis.

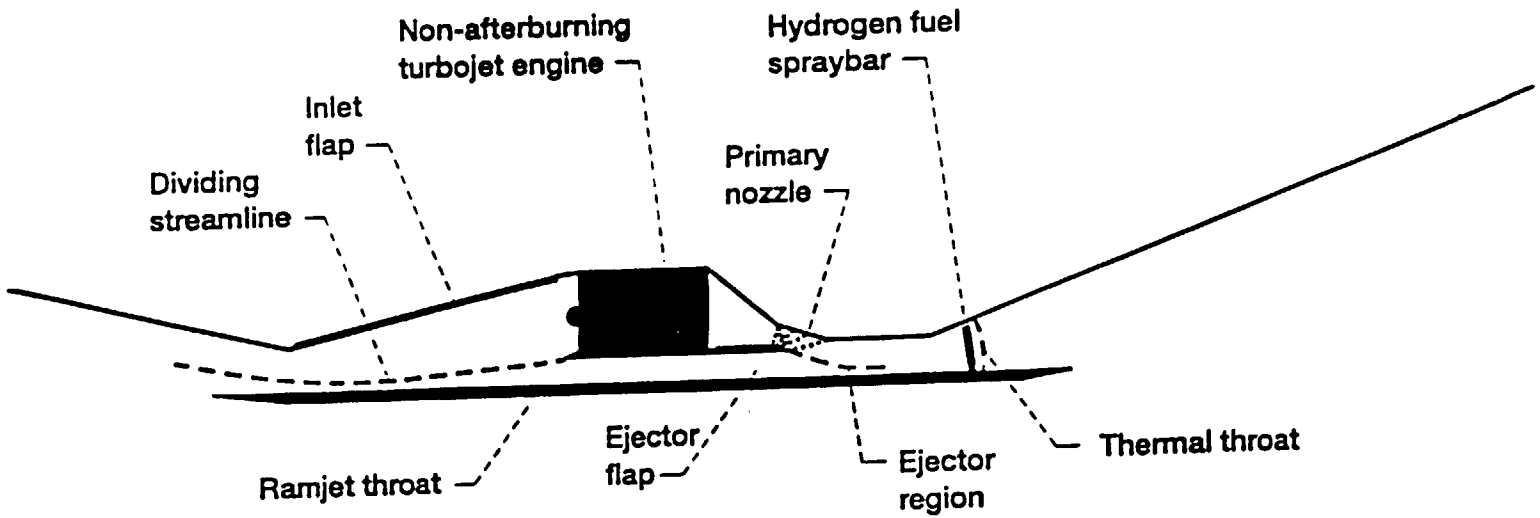

Figure 4.1 Features of TBCC Propulsion System (From Trefny and Benson)

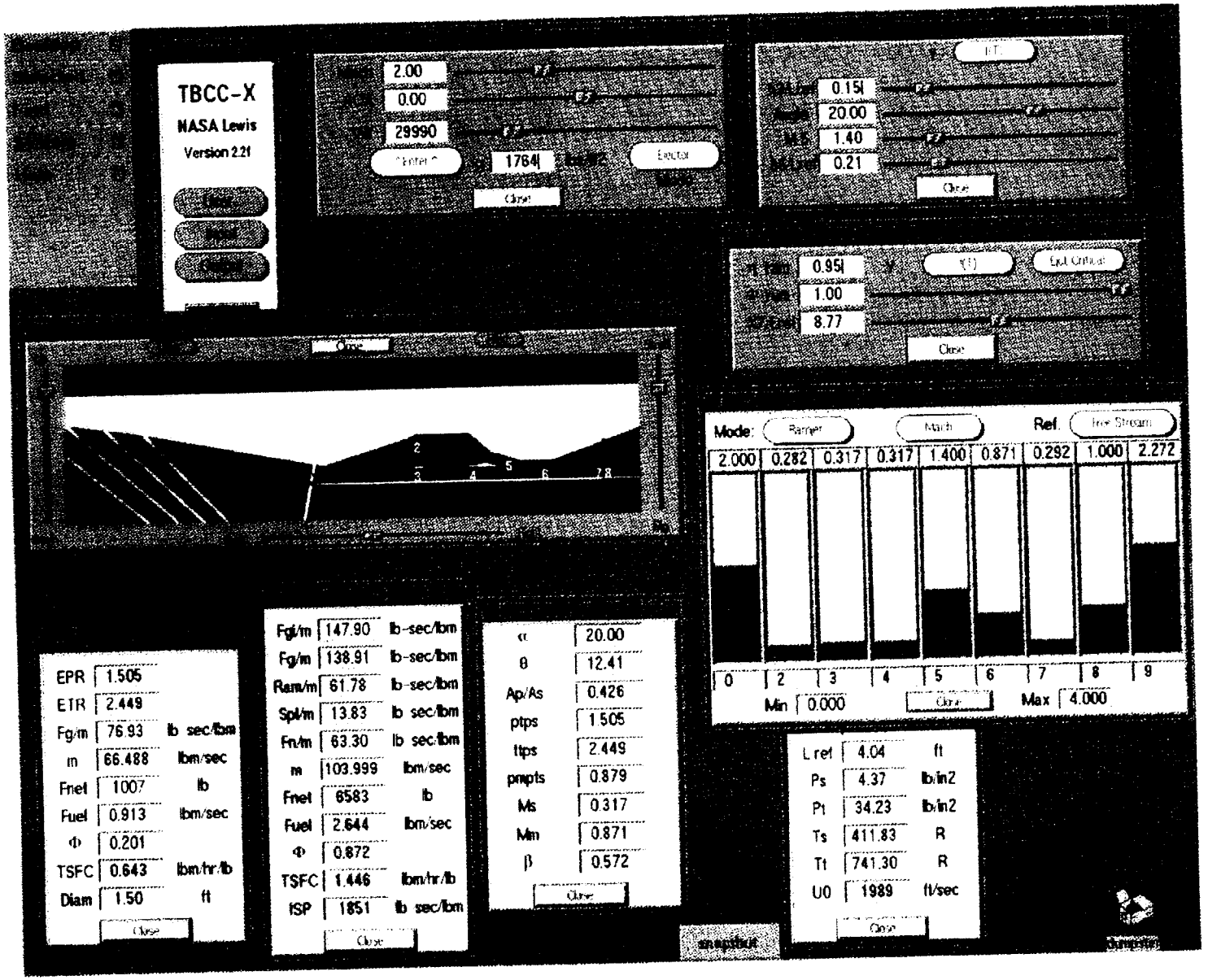

Figure 4.2 1-D TBCC Analysis of Pinf = 627 Psf, Tinf = 413R, M = 2.0 Case (From Trefny and Benson)

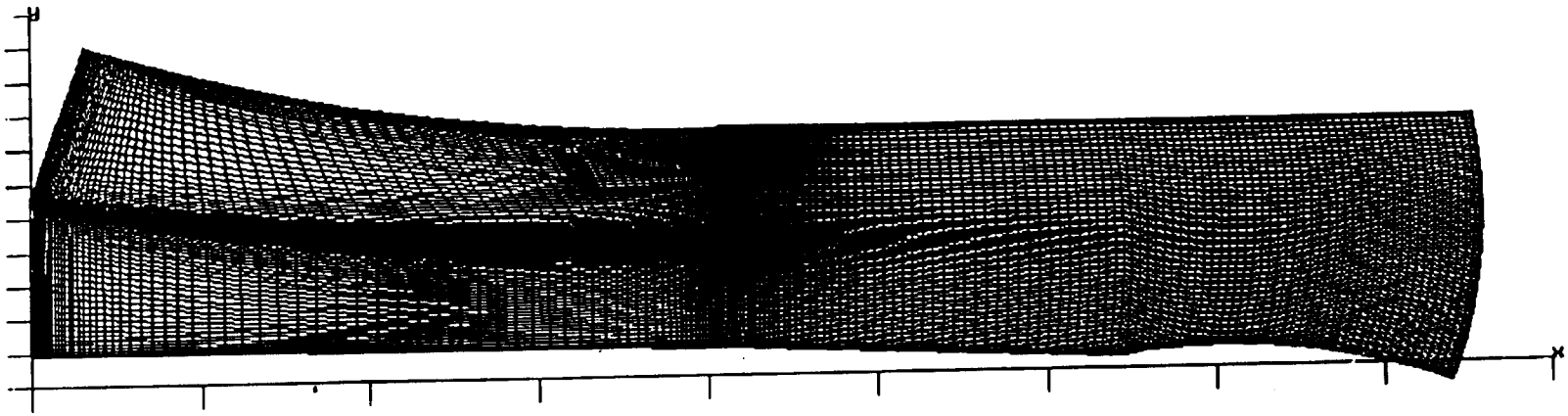

Figure 4.3 Grids for Turbojet - Ramjet Flow

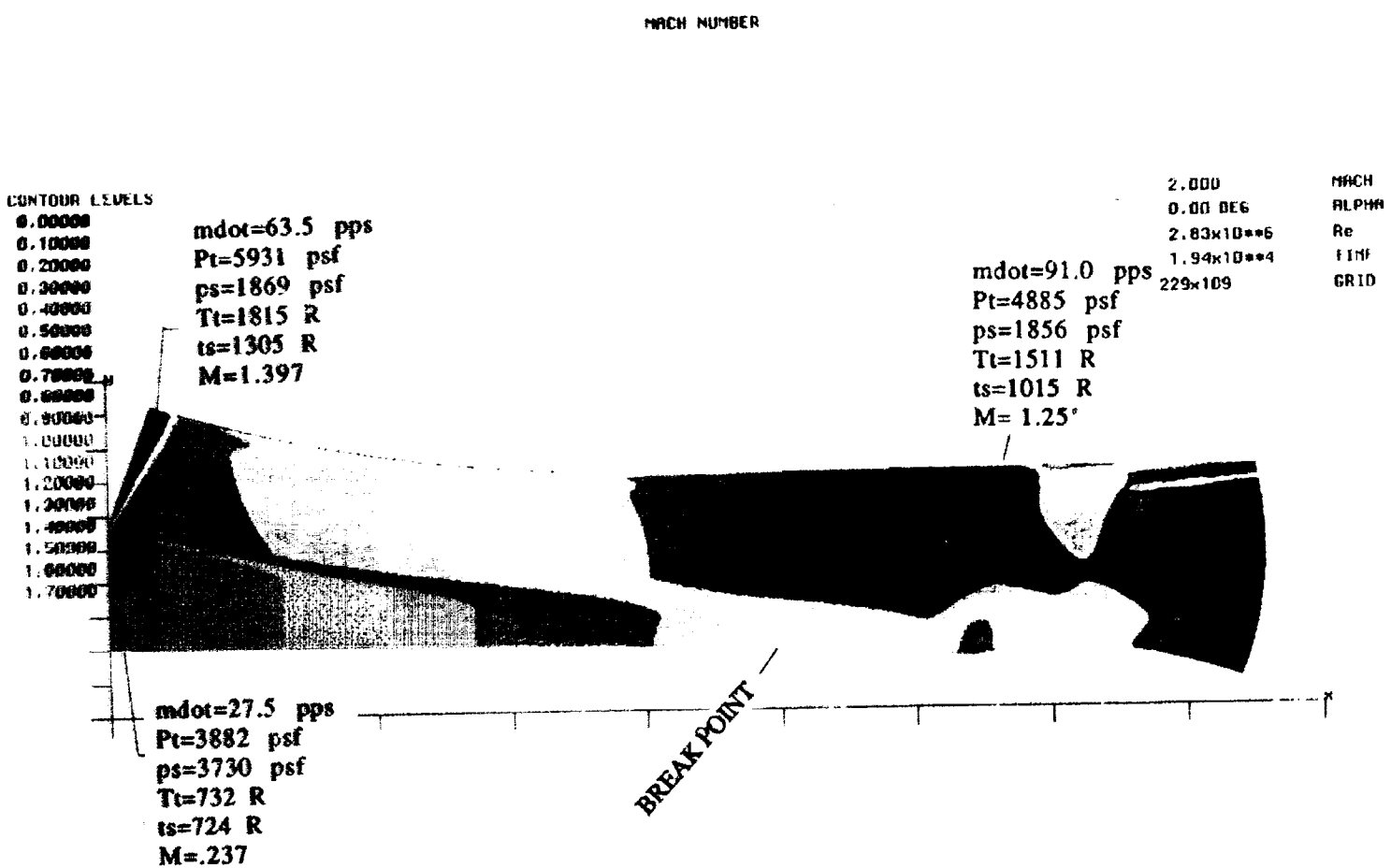

Figure 4.4 Mach Number Contour Plots Showing Converted Flow Properties at Mixed Condition

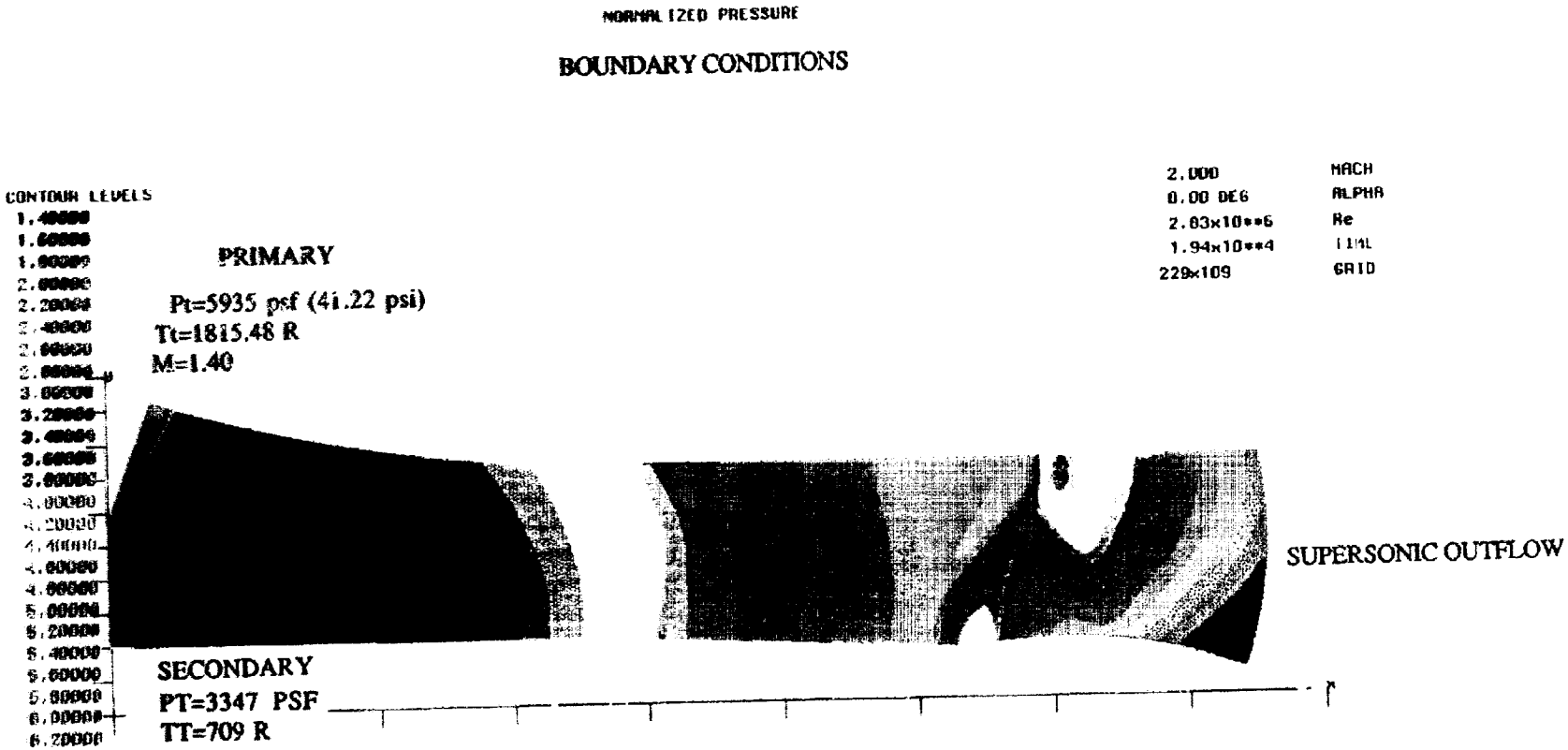

Figure 4.5 Normalized Pressures (Pinf = 627 psf) Contour Plots Showing Boundary Conditions

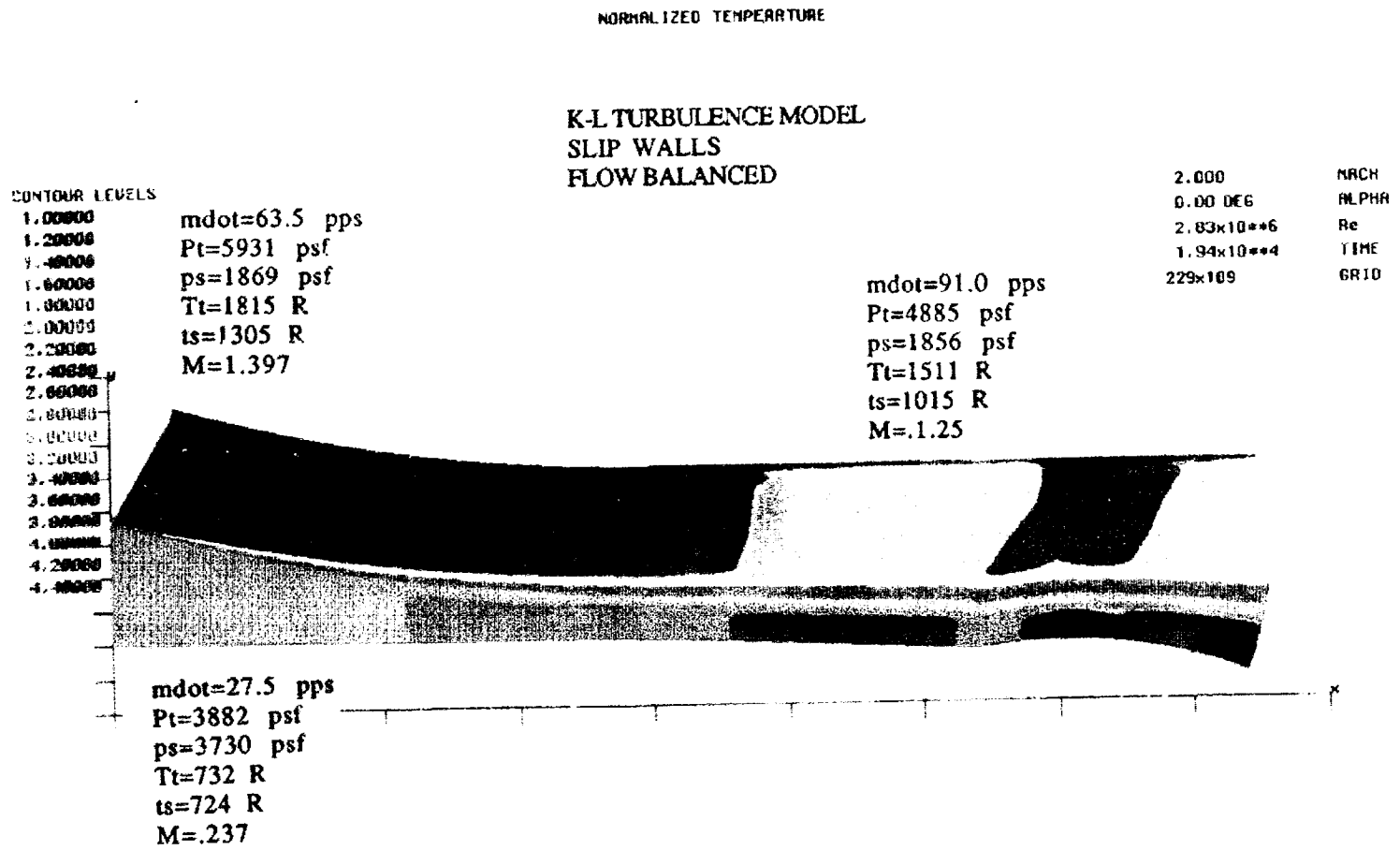

Figure 4.6 Normalized Temperatures (Tinf = 413R) Contour Plots

21 Feb 1996

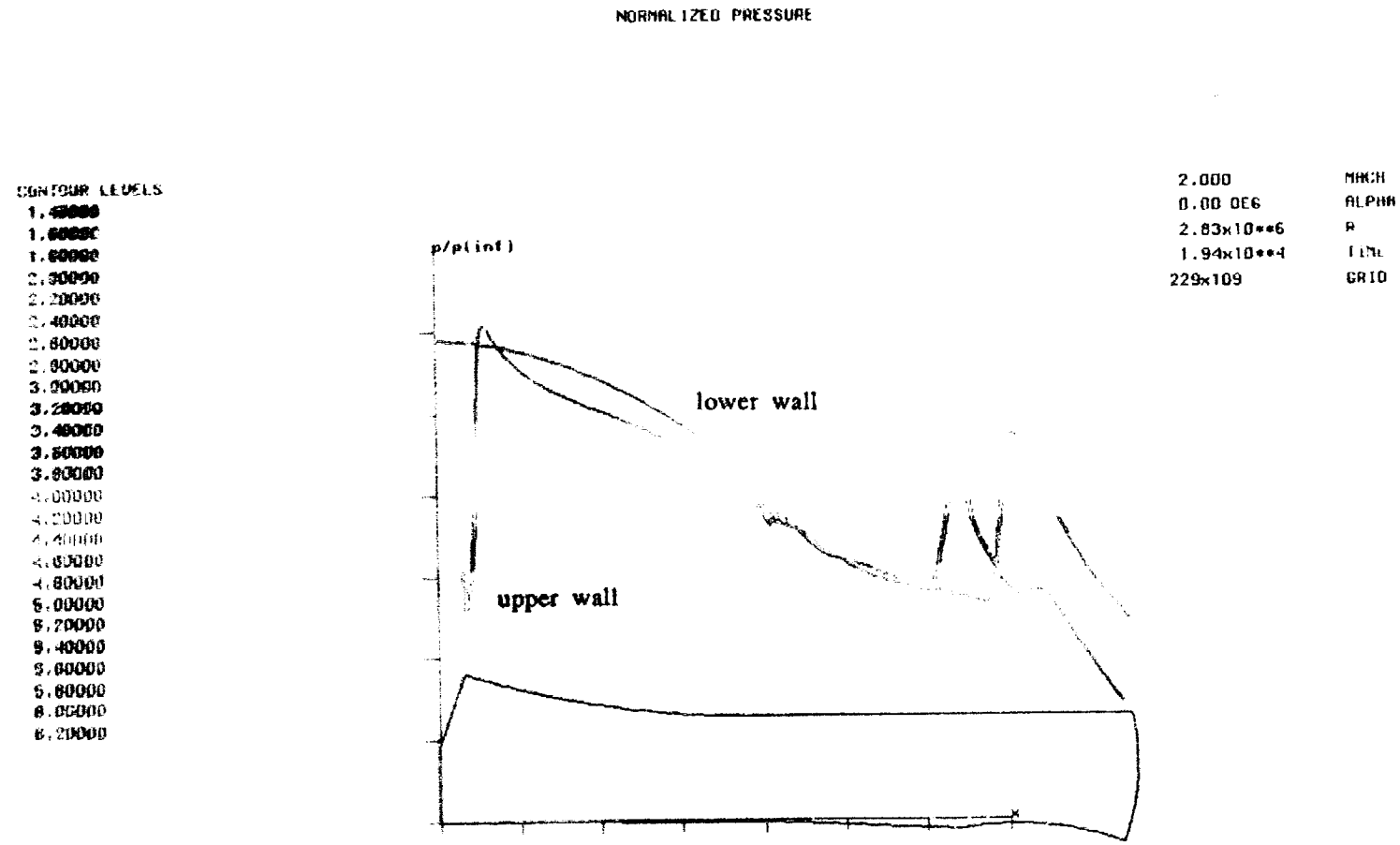

Figure 4.7 Upper and Lower Wall Normalized Pressures

PINF=627 TINF=413 M=2.00

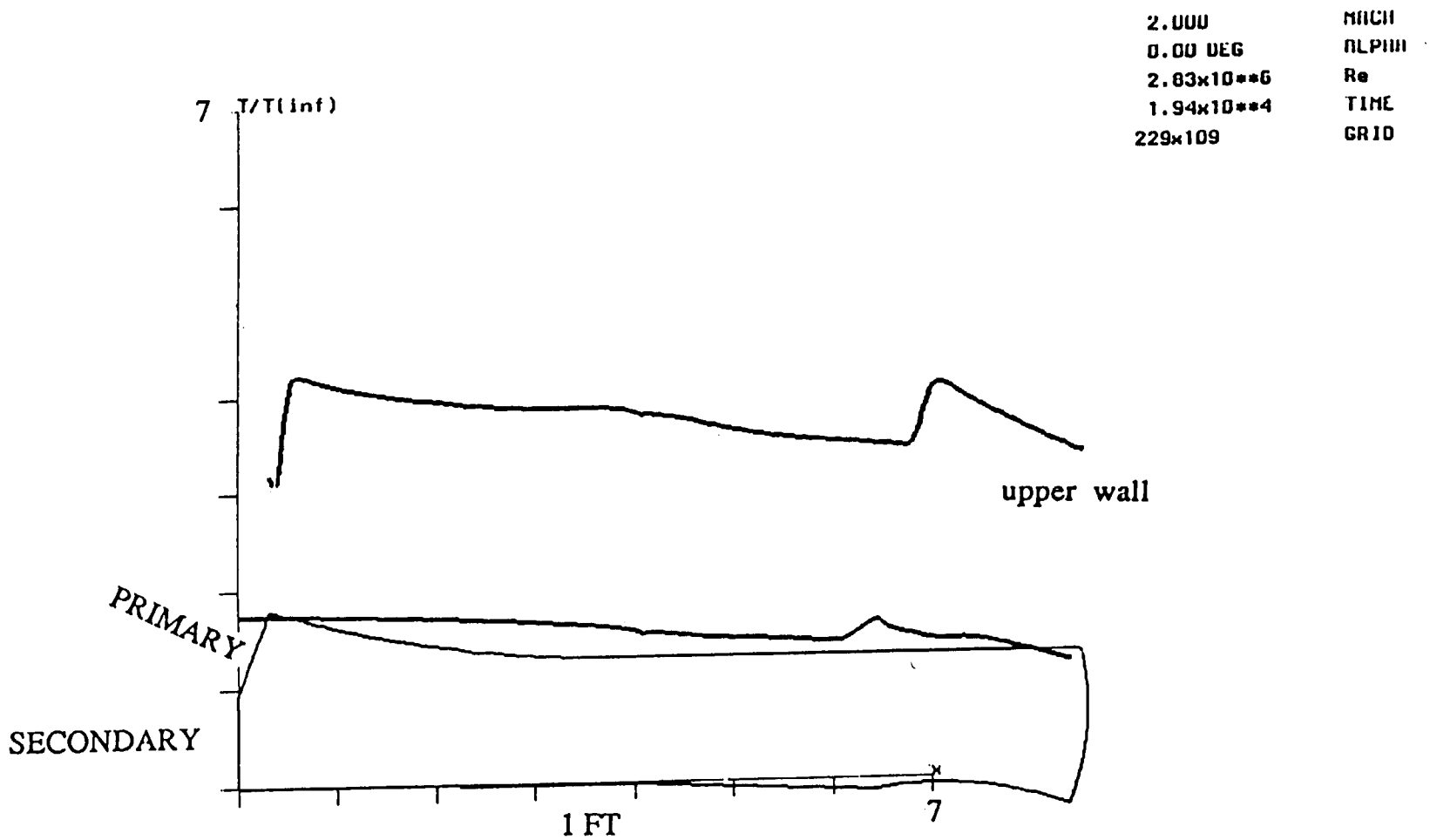

Figure 4.8 Upper and Lower Wall Normalized Temperatures

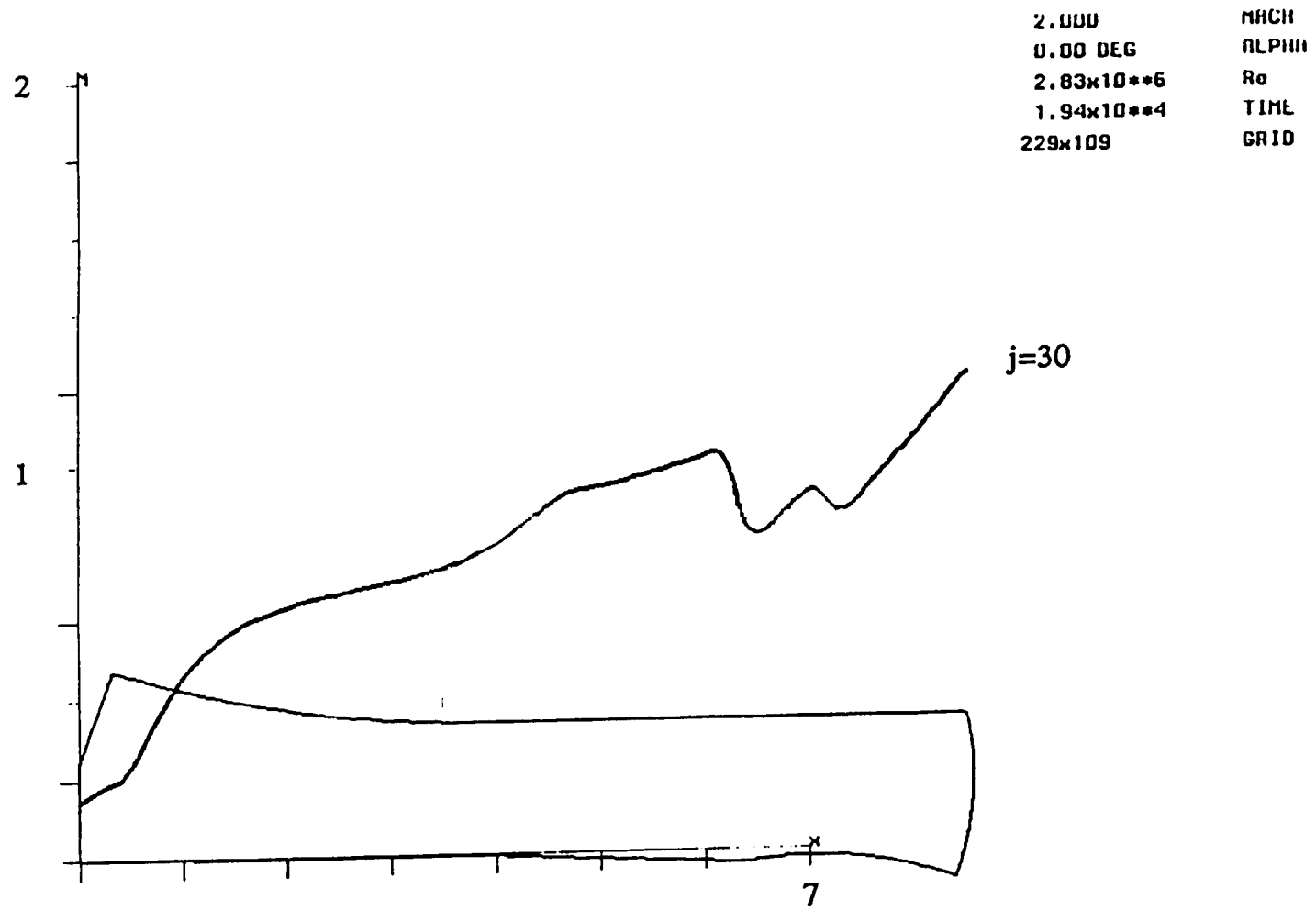

Figure 4.9 Mach Number Distribution in Secondary Stream (j = 30)

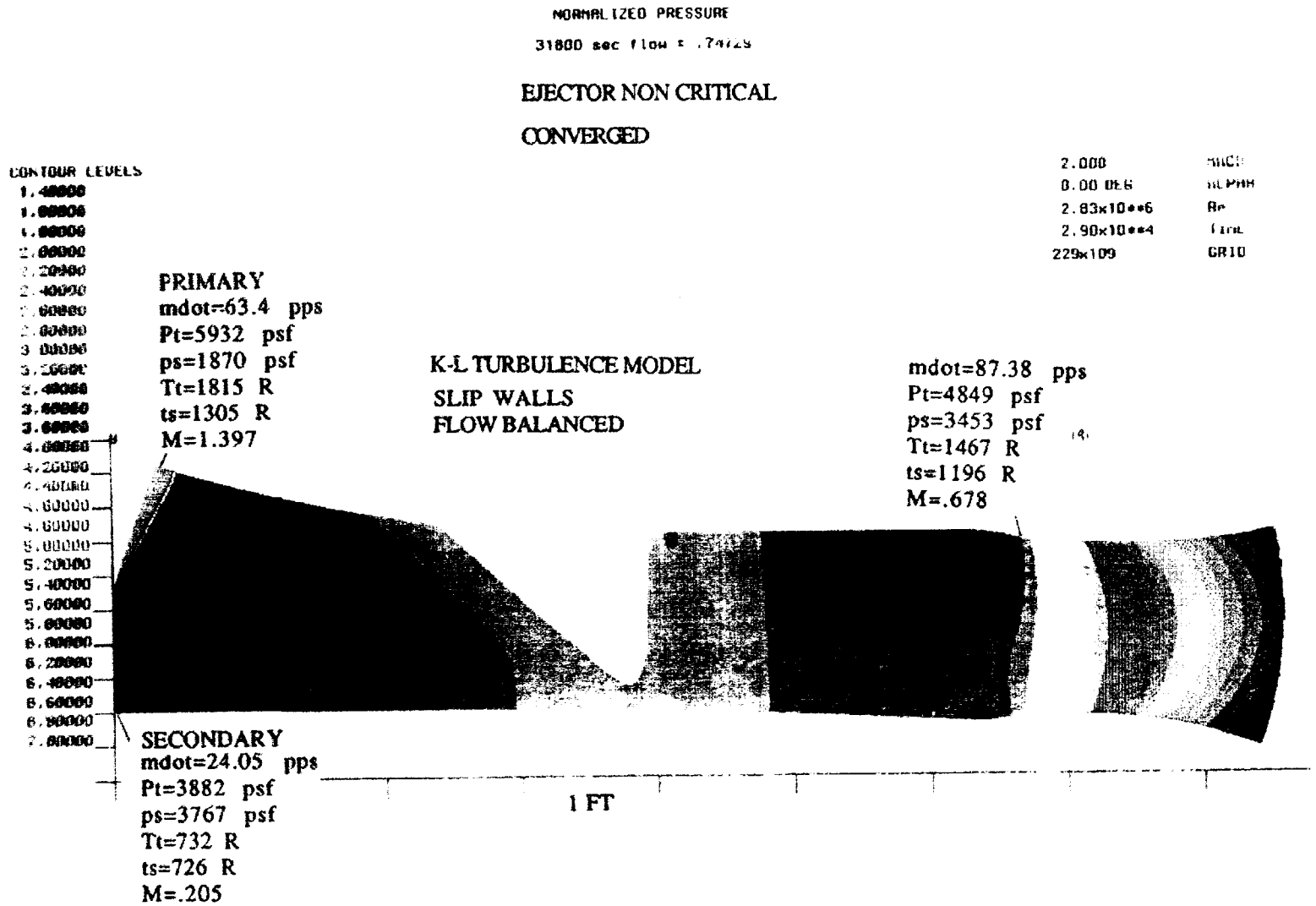

Figure 4.10 Non-Critical Flowfield as a Result of More Back Pressure - Normalized Pressures and CFDAveraged Pressures at Mixed Station (i = 191)

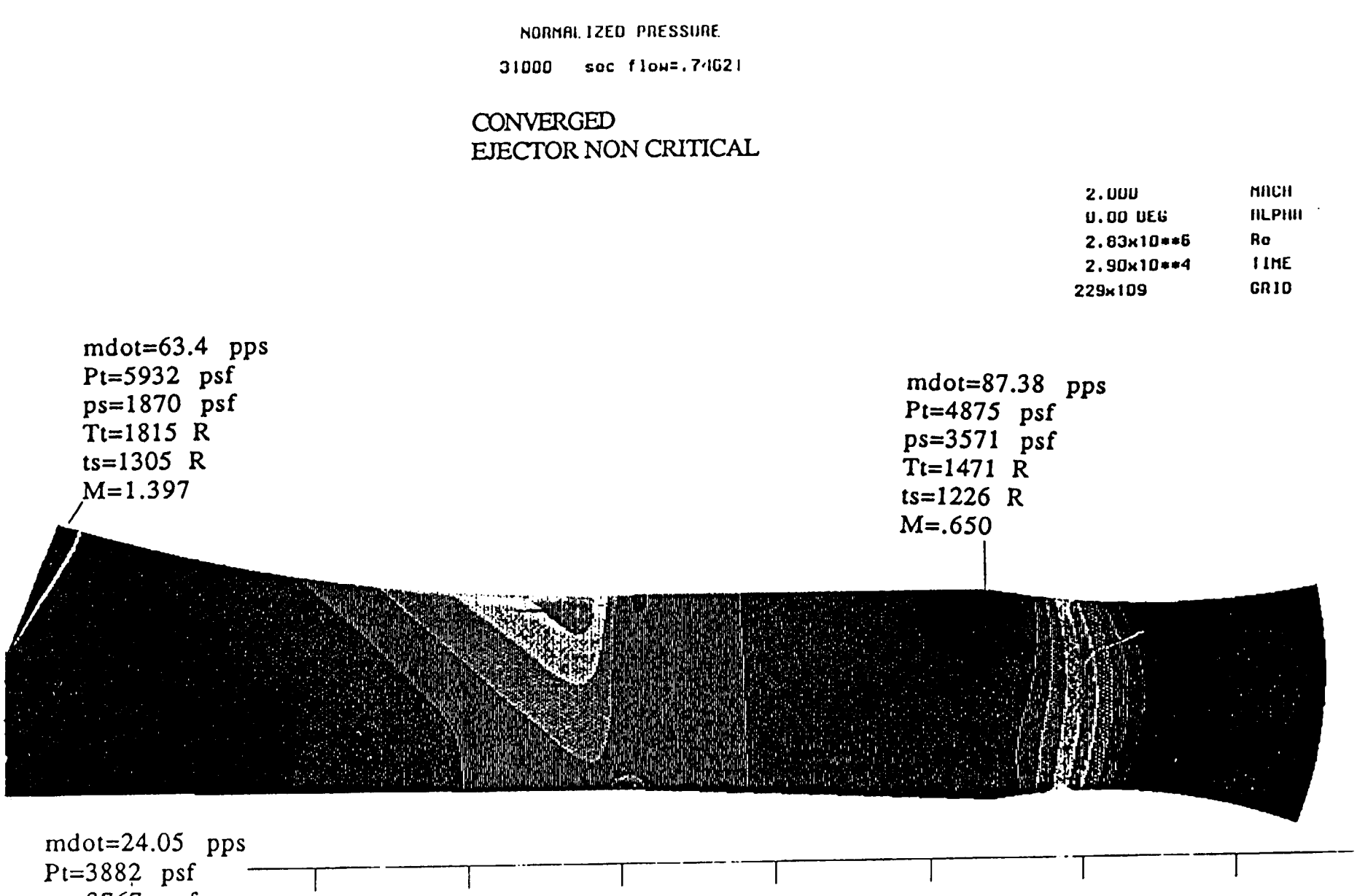

Figure 4.11 Non-Critical Flowfield as a Result of More Back Pressure-Normalized Pressures and CFD Averaged Pressures at Mixed Station (i = 184)

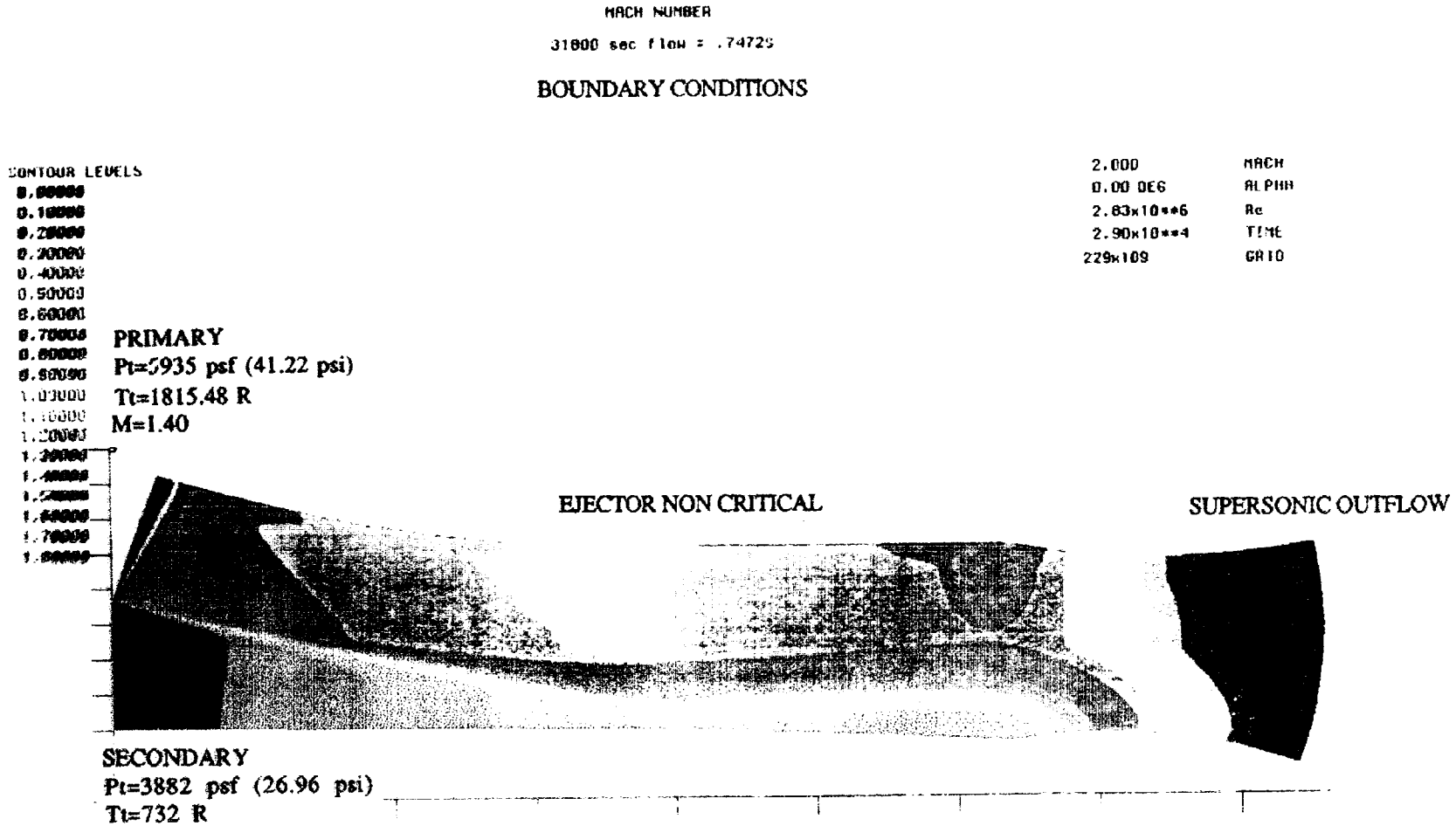

Figure 4.12 Mach Number Contours Showing Boundary Conditions

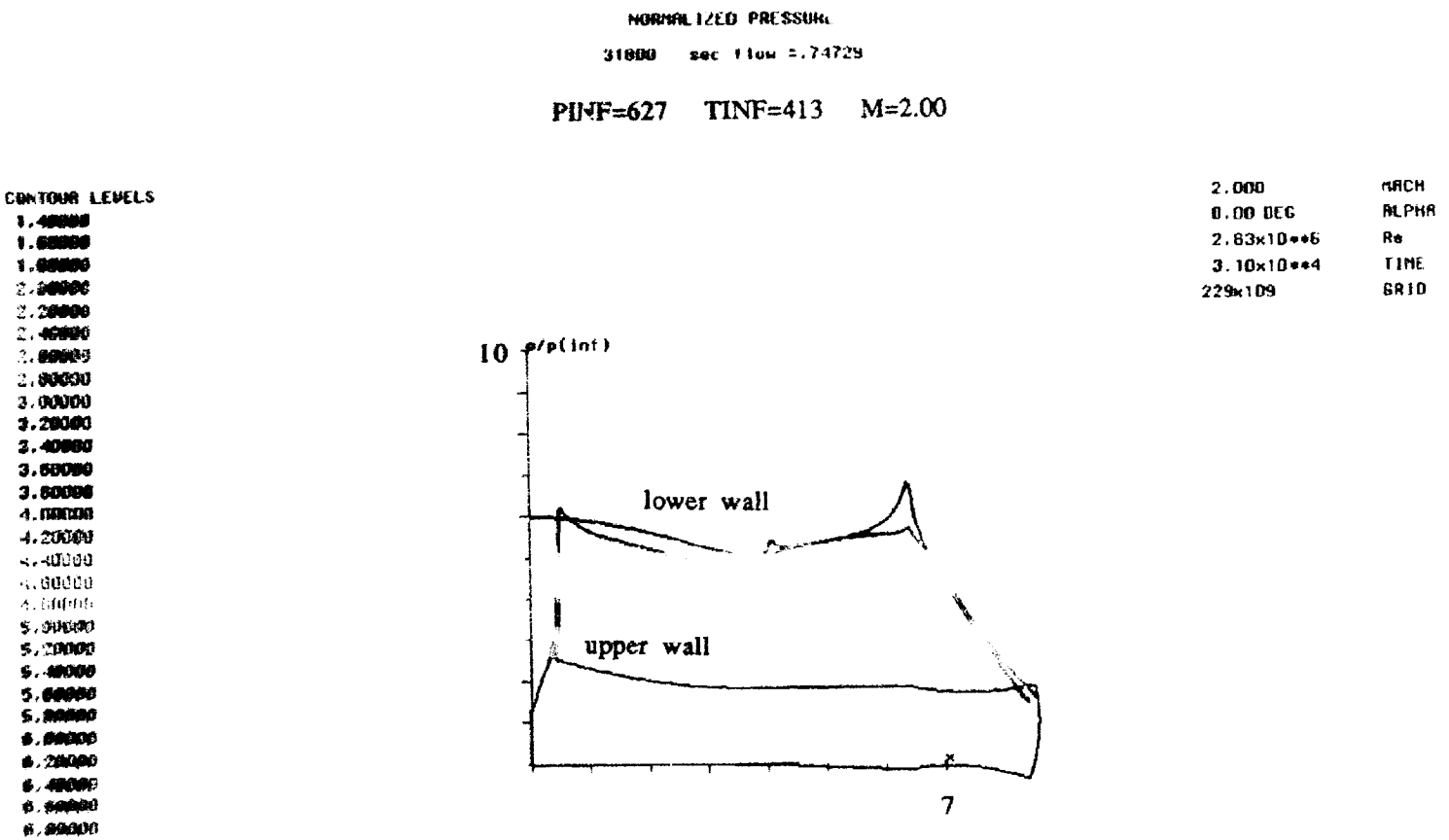

Figure 4.13 The Upper and Lower Normalized Wall Pressures

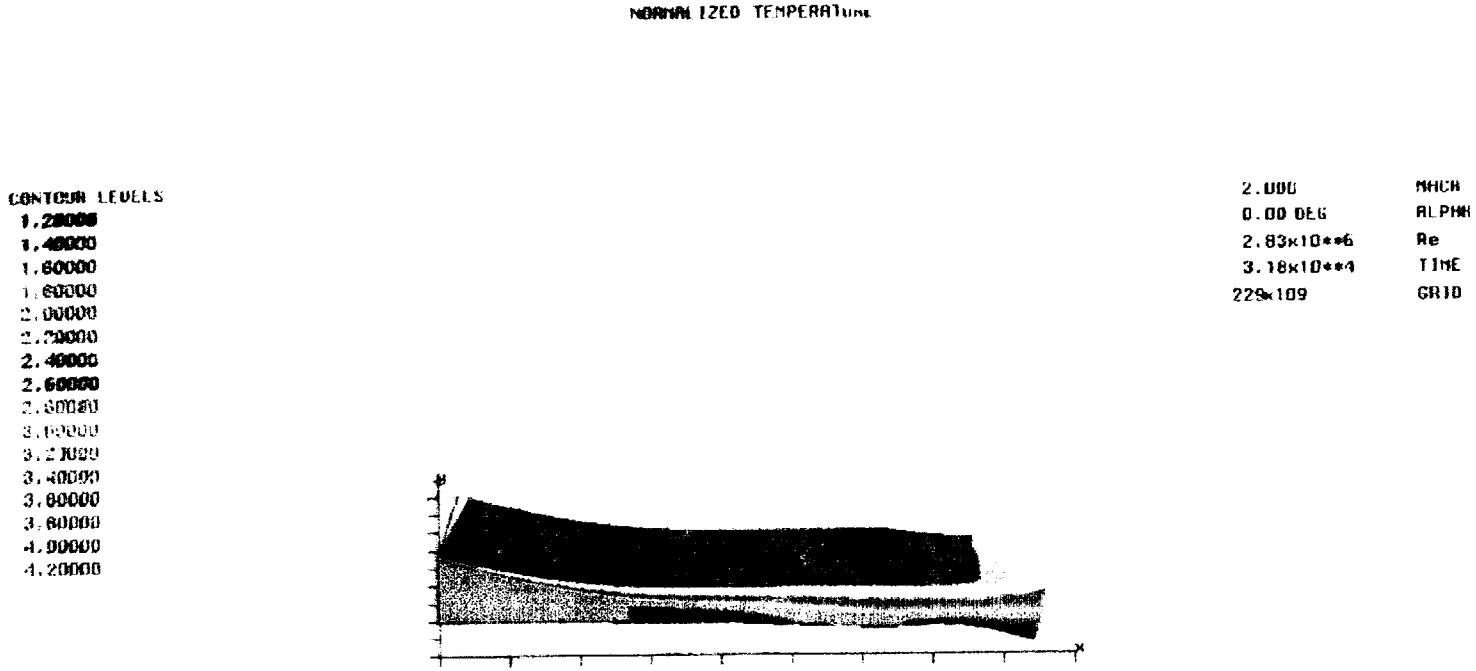

Figure 4.14 Temperature Contour Map

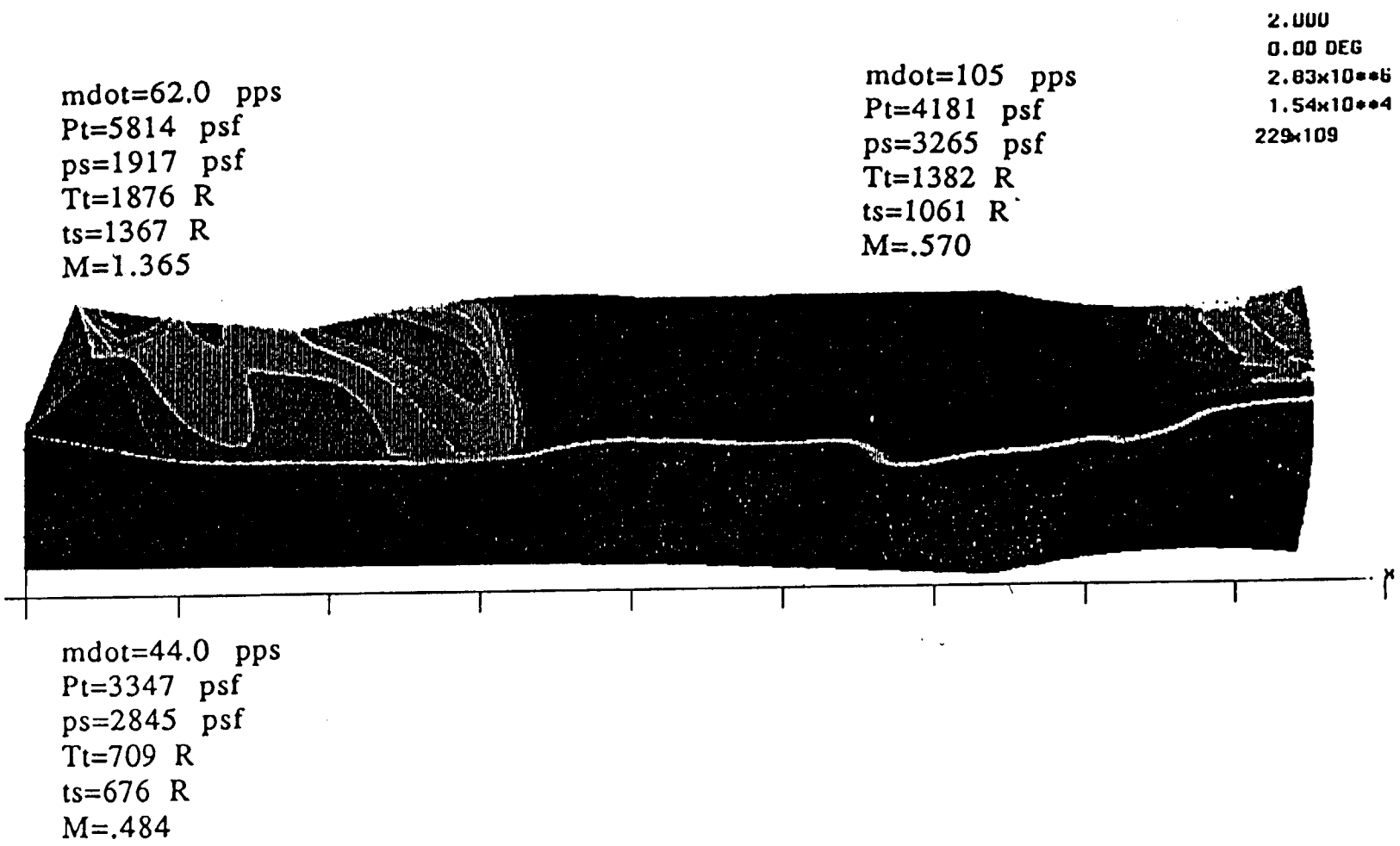

Figure 4.15 Normalized Temperature Map of Constant Area Geometry

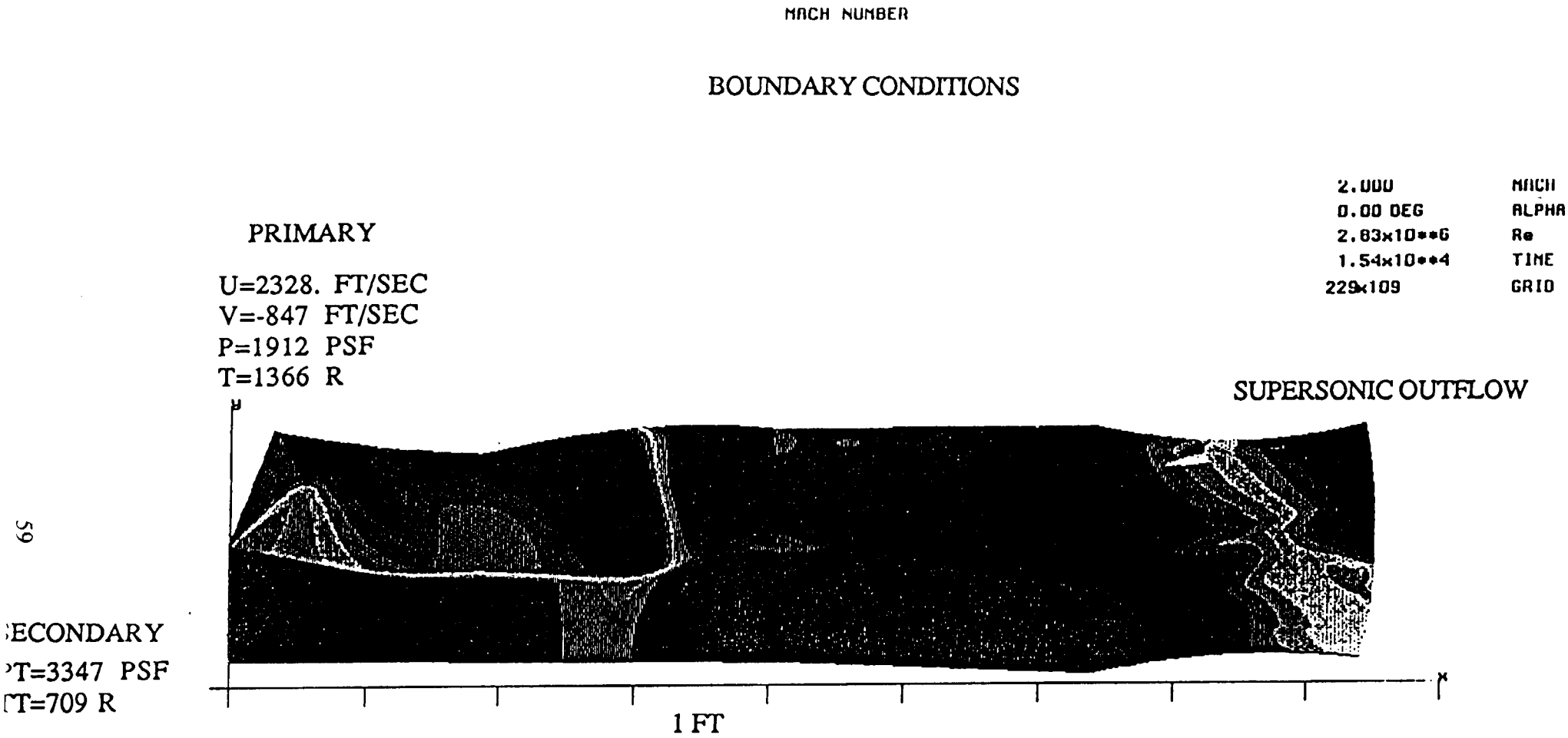

Figure 4.16 Mach Number Contour Map Showing Boundary Conditions

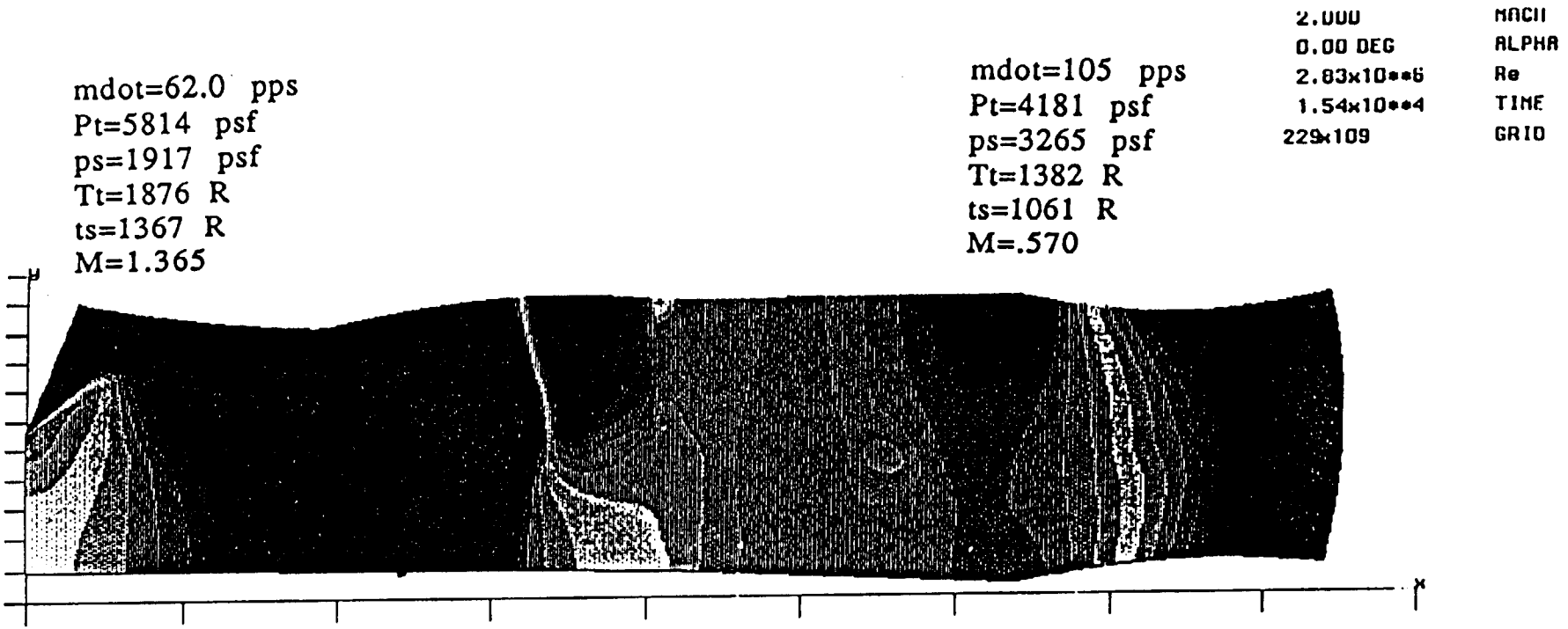

Figure 4.17 Normalized Pressure Map Showing Averaged CFD Results at the Exit Station (i = 229)

5. Conclusion

Two candidates of turbo-ramjet configurations for hypersonic vehicles were studied by CFD analysis. Conclusions for these studies were given in the previous chapters. Additional remarks related to the research work on supersonic airbreathing propulsion system are given in the following.

More research work should be done by using the NASA developed NPARC code with efficient grid generation software (such as GRIDGEN) to solve additional nozzle flow problems with complex geometry. If the test data are available for the given nozzle configurations, the research work can be used to conform the test results or further validate the NPARC code as a dependable CFD tool.

Extend the CFD study to supersonic nozzle with expansion ramp. The analysis will involve the interaction of internal flow and external flow. The objective of the research is to determine the effects of size and configuration variations of the expansion ramp on the thrust developed by nozzle.

Using a specific nozzle configuration as a reference, NPARC as a CFD tool, different two-equation turbulence models in the literature can be tested and compared. The turbulent flow is a nozzle could be very complex, it involves wall effects, free shear layers, reattaching flow, recirculation, fast expansion and shock wave compression, large temperature variation, and high turbulence intensities. Therefore, nozzle flow can give those turbulence models a rigorous test in all aspects. When experimental data are available for the nozzle, the most suitable turbulence model for nozzle flow may be obtained.

Future research effort could be focused on the CFD study of reacting flow inside supersonic combustor. Although there are codes developed by various NASA research centers, further validations are still desired. Improvement of these codes could include the radiation heat transfer effects, non-equilibrium processes, enhanced turbulence model, etc. With the improved CFD code, more realistic modeling for very complex flow problems, such as the TBCC propulsion system, can be studied.

6. Acknowledgments

This research was supported by the NASA Lewis Research Center under the grant NAG3-1500. The authors would like to thank Julian Earls, Sunil Dutta, Ed Meleason, Nick Georgiadis, Chuck Trefny, and Tom Benson for their help and support of this work. The authors would also like to thank Dean Dickman and Tracy Welterien of Lockheed Martin Tactical Aircraft Systems.

REFERENCES

1. Hagseth, P.E., et al., "Inlet and Nozzle Concepts for Advanced Airbreathing Propulsion Systems", Wright Labs Report WP-TR-92-3073, 1991.

2. Hansen, P., "Cold Flow Model Tests to Determine Static Performance of High Mach 2DCD and Sern Exhaust Nozzles", FluiDyne Report 1707/1725, 1990.

3. Cooper, G.K., and Sirbaugh, J.R., "PARC Code: Theory and Usage", Arnold Engineering Development Center Report AEDC-TF-89-15, December 1989.

4. Smith, B., "The KKL Turbulence Model and Wall Layer Model for Compressible Flows", AIAA 90-1483.

5. Chien, K.Y., "Predictions of Channel and Boundary Layer Flows with a Low Reynolds Number Turbulence Model", AIAA Journal, January 1982, volume 20, Number 1, pp 33-38.

6. Spezial, C.G., Ridha, A., and Anderson, E.C., "A Critical Evaluation of Two-Equation Turbulence Models for Near Wall Turbulence", NASA CR-182068, 1990.

7. Nichols, R.H., "Addition of a Two-Equation Turbulence Model to the Blocked PARC3D Code:, Calspan Corporation, AEDC Operations memorandum, October 28, 1991.

8. Back, L.H. and Cuffel, R.F., "Detection of Shocks in a Conical Nozzle with a Circular Arc Throat", AIAA Journal, Volume 4, Number 12, 1966, pp 2219-2221.

9. Addy, A.L., Dutton, J.C. and Anatucci, V.A., "Nonuniform Nozzle Flow Effects on Base Pressure or Supersonic Flight Speeds", AIAA Journal, Volume 24, Number 7, 1986, pp. 1209-1212.

10. Loth, E., Baum, J. and Lohner, L., "Formulation of Shocks Within Axisymmetric Nozzles", AIAA Journal, Volume 30, Number 1, 1992, pp 268-270.

11. Chang, I., Hunter, L.G., "Over-Under Nozzle CFD Study and Comparison with Data", 30th AIAA/ASME/SAE/ASEE Joint Propulsion Conference, June, 1994, AIAA-94-2949.

12. Benson, T.J., "Three-dimensional Viscous Calculation of Flow in a Mach 5.0 Hypersonic Inlet", AIAA 86-1461, June 1986.

13. Coltrin, R.E., "High-Speed Inlet Research Program and Supporting Analyses", Presented at Aeropropulsion '87 Conference, NASA Lewis Research Center, Cleveland, Ohio, November 17-19, 1987, NASA CP-10003.

14. Rose, W.C. and Perkins, E.W., "Innovative Boundary Layer Control Methods in High Speed Inlet System", Final Report, Phase I, SBIR Contract NAS3-25408, NASA Lewis Research Center, September, 1988.

15. Weir, L.J., Reddy, D.R., and Rupp, G.D., "Mach 5 Inlet CFD and Experimental Results, AIAA 89-2355, July, 1989.

16. Reddy, D.R., Benson, T.J., and Weir, L.J., "Comparison of 3-D Viscous Flow Computations of Mach 5 Inlet With Experimental Data", AIAA 90-0600, January, 1990.

17. Rose, W.C., Serafini, D.B., and Perkins, E.W., "Innovative Boundary Layer Control Methods in High Speed Inlet Systems", Final Report, Phase I, SBIR Contract NAS3-25783, NASA Lewis Research Center, November, 1991.

18. Trefny, C.J., Benson, T.J., "An Integration of the Turbojet and Single-Throat Ramjet", NASA Technical Memorandum 107085, Prepared for the 1995 Airbreathing Propulsion subcommittee Meeting Sponsored by the Joint Army-Navy-Air Force Interagency Propulsion Committee, Tamp, FL., 1995.

19. Addy, A.L.; Dutton, J.C.; Mikkelsen, C.D., "Supersonic Ejector-Diffuser Theory and Experiment", Report No. UILU-ENG-82-4001, Dept. of Mechanical and Industrial Engineering, University of Illinois at Urbana-Champaign, Urbana, IL., Aug., 1981.

20. Trefny, C.J., Benson, T.J., TBCC-X Code, Version 2.2f, NASA/Lewis, 1996.

21. Reed, C.L.," Central Difference Falcon User's Manual", Lockheed Forth Worth Company, CFD Group, June, 1994.